NASA CR-92231

CYCLIC & SUSTAINED LOAD FLAW GROWTH CHARACTERISTICS OF 6Al-4V TITANIUM

By

J. N. Masters

Prepared for

NATIONAL AERONAUTICS & SPACE ADMINISTRATION

July 1968

Contract NAS 9-7637

Technical Management

NASA Manned Spaceflight Center

Houston, Texas

S. V. Glorioso

Aerospace Group

THE BOEING COMPANY

Seattle, Washington

NASA CR-92231

FINAL REPORT

CYCLIC & SUSTAINED LOAD FLAW GROWTH CHARACTERISTICS OF 6AI-4V TITANIUM

By

J. N. Masters

Prepared for

NATIONAL AERONAUTICS & SPACE ADMINISTRATION

July 1968

Contract NAS 9-7637

Technical Management

NASA Manned Spaceflight Center

Houston, Texas

S. V. Glorioso

Aerospace Group

THE BOEING COMPANY

Seattle, Washington

CYCLIC & SUSTAINED LOAD FLAW GROWTH CHARACTERISTICS OF 6Al-4V TITANIUM

By

J. N. Masters

ABSTRACT

Plane-strain cyclic and sustained load flaw growth characteristics were evaluated for 6Al-4V titanium solution treated and aged forgings and weldment heat affected zones (HAZ). Cyclic load tests on both base metal and HAZ were performed at room temperature in air. Sustained load tests were performed on base metal in the environment of nitrogen tetroxide containing nitric oxide contents ranging from about 0.30 to 0.65 percent. These tests were performed at 70 and 90°F.

Results of cyclic flaw growth data obtained are presented as represented both by a least square fit of the data from forty-five data points, as well as a 99% lower confidence line of the data. It is shown that of three forging heats investigated, test scatter between heats is not important.

Results of sustained load tests in nitrogen tetroxide show that threshold stress intensity ratios increase steadily with increasing nitric oxide content. It is concluded from this series of tests that an increase in the existing lower limit of nitric oxide content (presently set at 0.40 percent by NASA specification MSC-PPD-2A) would be beneficial to service life of titanium vessels.

FOREWORD

During the last two years, a rather extensive study has been underway by NASA/Manned Spacecraft Center, Houston Texas, to assess and assure the structural integrity of Apollo structure. Since several 6Al-4V titanium pressure vessels are involved, and since ground failures of two of these vessels have been experienced, considerable effort has been devoted to the development of data applicable to these vessels and to the several environments to which they are exposed. As part of this effort, NASA in 1966 requested the Space Division of The Boeing Company to perform an investigation of flaw growth characteristics of 6Al-4V titanium tankage material. This original work, performed under NASA Contract 9-6665 dealt primarily with sustained load flaw growth in various environments. The program reported herein, was performed under NASA Contract NAS 9-7637 and deals primarily with cyclic load flaw growth. A second phase dealt with the sustained load flaw growth behavior in an environment of nitrogen tetroxide containing varying levels of nitric oxide. Period of performance was October 26, 1967 thru July 1, 1968. The work was administered under the direction of Mr. S. V. Glorioso at NASA/MSC.

Boeing personnel who participated in the investigation include C. F. Tiffany, Program Supervisor, and J. N. Masters, Technical Leader. Structural testing of specimens was conducted by A. A. Ottlyk and G. E. Van Staalduine.

The information contained in this report is also released as Boeing Document D2-114298-1.

SUMMARY

The objective of this program was to investigate cyclic flaw growth of 6Al-4V S.T.A. titanium alloy and the effect of nitric oxide content on the threshold for constant stress flaw growth of this material in nitrogen tetroxide. Tests were performed on uniaxially loaded pre-cracked surface flawed specimens from several different forgings. Sustained load tests were performed at test temperatures of 70 and 90°F in nitrogen tetroxide containing nitric oxide contents of about 0.30 thru 0.65 percent by weight. Cyclic tests were all performed in an environment of room temperature air.

Results of the cyclic tests are plotted in terms of stress intensity ratio versus growth rate. Both nominal curves and lower 99% confidence curves are shown. The effect of minimum to maximum cyclic stress (R value) is shown as a plot of relative cyclic life versus R value.

Results of the sustained load tests showed that threshold values increase slightly with increasing nitric oxide content at both test temperatures. Additionally, it was found that of two forgings used in these tests, threshold ratios (i.e., K_{Ii}/K_{Ic} values below which growth did not take place) were similar, even though the actual K_{Ic} values for the two forgings were quite different.

TABLE OF CONTENTS

LIST OF ILLUSTRATIONS

LIST OF TABLES

1.0 INTRODUCTION

Many failures in pressure vessels have originated at flaws. Some failures have occured in proof tests of pressure vessels. Proof test failures result where the size of a flaw is sufficiently large to become unstable before proof stress is attained or at proof stress (during a hold period) if the threshold stress intensity is exceeded. Operational failures have often occured after a flaw grew sufficiently in size to become unstable at the operating stress. An estimate of the performance capability of pressure vessels requires knowledge of initial flaw sizes, critical flaw sizes, and subcritical flaw growth characteristics of the vessel material.

In a previous investigation (Reference 1) emphasis was placed on development of sustained load behavior of 6Al-4V S.T.A. titanium alloy in several liquid environments. This included some tests in nitrogen tetroxide with a fixed nitric oxide level within the MSC specification MSC-PPD-2A. For background information and more detailed discussion of analytical techniques, the reader is referred to the final report of the Reference 1 study.

The investigation reported herein was undertaken to:

1. Investigate sustained load subcritical flaw growth behavior in nitrogen tetroxide containing varied nitric oxide contents.

2. Investigate cyclic load flaw growth behavior as affected by varied forging heats, and by varied minimum-to-maximum cyclic stress levels.

2.0 MATERIALS

2.1 TITANIUM FORGINGS & WELDMENTS

Base metal specimens tested in this program were machined from each of four 6Al-4V titanium forgings. One of these, supplied by Aerojet General Corporation (AJG) Downey, California, was a solid motor case cylindrical forging. This forging was produced by Cameron Iron Works. Composition, heat treat, and tensile data are shown in Table I. The remaining three forgings were parts of finish machined and heat treated Apollo SPS fuel and oxidizer cylindrical sections. All base metal specimens (with the exception of one series) were machined such that loading was parallel to the hoop direction. All Apollo tank material was solution treated and aged at 1100°F for 9 hours, plus stress relieved at 1000°F for 4 hours.

Welded specimens were machined from a girth weld taken from an Apollo SPS oxidizer tank assembly. These specimens were machined such that loading was perpendicular to the weld centerline.

A summary of forging and weldment used in the various test series is shown in Table II.

2.2 TEST FLUIDS

As shown in Table II, one series of sustained load tests was performed in nitrogen tetroxide containing varied levels of nitric oxide. Nitrogen tetroxide was prepared and used in four separate samples, as shown in Table III. These samples were prepared by transferring oxidizer directly from a single field storage tank to either a two-gallon or five-gallon transfer vessel. Nitric oxide content of the field supply was less than 0.10%. Nitric oxide gas was then added incrementally to the transfer vessels until the desired level of NO was approached.

NO content of the first two samples prepared (samples A and C) was measured only once. On samples B and D, several readings were taken during the course of testing for determination of both water content and NO level. Representative values are shown below Table III.

3.0 PROCEDURES

3.1 SPECIMEN FABRICATION

Precracked surface flaw specimens were used for all static toughness, sustained load, and cyclic tests. Flaws were made by electric discharge machining (EDM) a starter notch, and extending the notch by low stress tension fatigue. The fatigue extension was accomplished at a maximum gross stress of 30 Ksi at 1800 cpm. From 6000 to about 25,000 cycles were required, depending upon initial notch dimensions. All precracking was done in air at room temperature. Material for all specimens was supplied in the fully heat treated condition (i.e., solution treated, aged and subsequently stress relieved).

Overall dimensions for the surface flawed specimens were tailored to the size and shape of available material. Thickness of the AJG forging was sufficient to allow the use of flat specimens, Figure 1. Additional series of AJG specimens were tested under cyclic loading with reduced thickness, and with both reduced thickness and gage widths to check these variables.

Tests of Apollo tank cylinder materials utilized specimens of the configuration shown in Figure 2(a). A secondary series of tests was performed with different loading direction (See Figure 2(b)) and with varied gage width (0.50 - and 0.80-inches) to check these variables. Thickness of all of these specimens was as-received representing final vessel wall thickness.

Welded specimens, shown in Figure 3 were machined flat in the gage area to provide the thickest possible uniform and flat section. Surface flaw was located approximately 0.020-inches away from the intersection of the fusion line with the surface in the heat affect zone. This location was selected on the basis of test results of Reference 1. These tests indicated that crack initiation occurred most readily in the weld centerline, followed closely by the location selected. This location was selected because applied stresses are higher at this point.

3.2 FLAW GROWTH TEST SETUP

The sustained load test specimens were loaded in 10,000 lb. dead-load creep machines. Those tests using nitrogen tetroxide utilized a setup as shown in Figure 4, 5, and 6. Liquid was contained in two pressurized tanks connected with flex lines to each other and to a small cup clamped to the test specimen. Periodically, one of the tanks was raised or lowered so that the fluid would flow through the specimen cup thus supplying fresh liquid. Temperature was controlled by warm air supplied from Coates heaters. A schematic of the fluid and pressurization system is shown in Figure 7.

Cyclic tests were performed in an environmentally controlled laboratory at the Boeing Developmental Center in a Tinnius Olsen universal tensile machine of 20,000 lb. capacity.

3.3 EXPERIMENTAL APPROACH FOR SUSTAINED AND CYCLIC LOAD TESTS

The approach used to define threshold stress intensity levels is shown schematically in Figure 8. The first surface flawed specimen (after determining the static K_{Ic} value) was loaded to a target stress intensity level less than critical (i.e., an initial stress intensity value, K_{Ii}). The specimen was held at constant load until failure or for a predetermined time (usually 24 to 48 hours). If failure did not occur, the specimen was cycled in air in low stress fatigue to mark the flaw front, and then was pulled to failure. Evidence of sustained load growth was then observed by a separation between the initial fatigue crack extension and that of the final marking. With either failure or evidence of growth in the first specimen, subsequent specimens were loaded at successively lower K_{Ii} values until neither failure nor growth took place. Usually, the threshold value was bracketed with three to four specimens.

Cyclic tests were performed by programming several series of tests involving several combinations of initial flaw sizes and maximum applied stress. The general approach is shown schematically in Figure 9. Generally, three values of applied stress (σ_1, σ_2, and σ_3) and three values of initial flaw size $(a/Q)_1$, $(a/Q)_2$, and $(a/Q)_3$ were used. Majority of tests were targeted at initial stress intensity values of about 75% of critical by using combinations of $\sigma_3 \times (a/Q)_1$, $\sigma_2 \times (a/Q)_2$, and $\sigma_1 \times (a/Q)_3$. Variations from these were then accomplished by using other combinations of flaw size and maximum stress to develop other stress intensity ratios. In all cases, cycling was continued, at approximately 5 to 10 cpm, until failure. Upon failure, the initial stress intensity value was calculated using initial flaw size as measured from specimen photographs. Critical flaw sizes were not normally sufficiently well defined to allow accurate calculation of K_{Ic} values.

3.4 STRESS INTENSITY SOLUTIONS

Initial and critical stress intensity values for flat specimens (i.e., flat in the direction of loading) were calculated using the expression:

$$K_I = 1.1\sigma \sqrt{\frac{\pi a}{Q}} \quad M_K$$

Values for Q and M_K are shown in Figures 10 and 11. Kobayashi's M_K term (the upper curve of Figure 11) was used for all specimens where a/2c values were 0.29 or less; Smith's M_K term was used for a/2c values of 0.33 and greater; and an average M_K value between these limits was used for intermediate shapes. Attempt was made to control a/2c value to 0.25 or less.

Stress intensity values for curved specimens (i.e., of the type shown in Figure 2a) were calculated using the expression:

$$K_I = 1.1\ \sigma_T \sqrt{\frac{\pi a}{Q}}\ M_K + M_B\ \sigma_B \sqrt{\frac{\pi a}{Q}}$$

where

σ_T = uniform gross tension stress, Ksi

σ_B = extreme fiber bending stress, Ksi

Values of M_B are shown in Figure 12. The relationship of bending-to-tension stress as determined in Reference 1 is shown in Figure 13.

4.0 TEST RESULTS

4.1 MECHANICAL PROPERTIES

Room temperature tensile and 0.2% yield strength of the AJG forging are 172.5 and 160.6 Ksi, respectively. These values represent the average of three tests. The average of two tests of weldments were 135.2 Ksi tensile and 127.3 Ksi yield strength. Yield strength could not be measured on the thin propellant tank material because of the curvature; a value of 155 Ksi was used in calculating stress intensities. Any error in using this assumed value should be less than one percent.

4.2 PLANE STRAIN FRACTURE TOUGHNESS

Plane strain toughness values were determined at room temperature for the four forgings and the one weldment. A summary of the values obtained is shown in Table IV. Included in the table are four data points from Reference 1 for the two Apollo fuel cylinder forgings.

The average K_{Ic} values for the four forgings range from 41.9 to 48.6 Ksi $\sqrt{\text{in.}}$ while the average weld HAZ value is 44.7 Ksi $\sqrt{\text{in.}}$

4.3 SUSTAINED LOAD FLAW GROWTH

Sustained load subcritical flaw growth studies were performed with combinations of the two Apollo fuel cylinder forgings and four batches of N_2O_4 (Reference Tables II and III). Tests were run at either 70° or 90°F. Test parameters and results are included in Tables V and VI. These tables include specimen dimensions, initial flaw size, test time and temperature, calculated initial stress intensity values, and applied stress intensity ratios. These ratios represent the applied initial stress intensity, K_{Ii}, divided by the respective average K_{Ic} value as determined from static tests. Failure occurred in two test runs (i.e., specimen number 1-15 and 2-26). On the remaining specimens, amount of growth (in terms of percent increase in flaw depth) is shown.

4.4 CYCLIC LOAD FLAW GROWTH

Cyclic load subcritical flaw growth studies were performed on three different forgings and one weld metal sample (Reference Table II).

Cyclic Test Series I (Baseline)

Table VII shows test parameters and results for the baseline tests using the Aerojet forging, and a minimum to maximum cyclic stress ratio of 0.10 (i.e., R = 0.10). Nominal gage thickness and width of all of these specimens were 0.100 x 0.800 inches (see Figure 1). Actual dimensions, measured initial flaw sizes, applied cyclic stress, calculated K_{Ii} values, max K_{Ii}/K_{Ic}

ratios, and cycles-to-failure are shown in the table. An average K_{Ic} value of 45.8 Ksi $\sqrt{In}$ was used in all cases to determine the stress intensity ratio. The data of Table VII are plotted in Figure 14 in terms of K_{Ii}/K_{Ic} ratios versus cycles to failure. Different maximum stress levels are shown by different symbols as noted in the figure. Solid curves shown in Figure 14 represents a best fit least square curve for the obtained data and a lower confidence band. Details on construction of these curves are included in Section 5.2.

Cyclic Test Series II

The second series of cyclic tests was performed with material from Apollo Fuel Cylinder #2 (See Table II) and under the same test conditions as that of the baseline tests (i.e., room temperature air environment and R = 0.10). Nominal gage thickness and width of all of these specimens were 0.056 x 0.500 inches (See Figure 2a). Actual dimensions, measured initial flaw sizes, applied cyclic stress, calculated K_{Ii} values, maximum K_{Ii}/K_{Ic} ratios, and cycles-to-failure are shown in Table VIII. An average K_{Ic} value of 41.9 Ksi $\sqrt{In}$ was used in all cases to determine the stress intensity ratio. The data of Table VIII are plotted in Figure 15 in terms of K_{Ii}/K_{Ic} ratios versus cycles to failure. The solid curve superimposed in the figure represents the baseline test curve. As shown in this figure, all data points fall short of the baseline curve.

Cyclic Test Series III

This series of tests was performed using material from Apollo Oxidizer Cylinder #1, and under the same test conditions as that of the baseline tests (i.e., room temperature air environment and R = 0.10). Nominal thickness was 0.065 inches, specimen width was varied from 0.50 to 0.80-inches, and tests were performed in both directions ("L" and "T" directions) as shown in Table IV. Note that specimen curvature with respect to direction of loading is involved in the "L" specimens. Test data is included in Table IX and is plotted in Figure 16. K_{Ic} values of 47.3 and 43.0 Ksi $\sqrt{In}$ in the "L" and "T" directions, respectively, were used to calculate stress intensity ratios. While the points as plotted in Figure 16 generally fall to the left of the baseline curve, there is no major effect in cyclic life of the specimen width and test direction variables. It is possible that errors are involved in the stress intensity solution for curved specimens, however, such errors would tend to be minimized when data is plotted in terms of stress intensity ratios instead of actual applied K_{Ii} values.

Cyclic Test Serie IV

This series of tests was programmed primarily to check thickness effects, and also to provide a second check on specimen width effects. Accordingly, the

baseline forging (i.e., Aerojet forging) was used but thickness was reduced to 0.060. Specimen width again was controlled to values of 0.50- and 0.80-inches. Raw data is included in Table X and the results are plotted in Figure 17. As would be expected, the reduced thickness results in a reduction in cyclic life; specimen width within the range tested has little if any effect.

Cyclic Test Series V

This last series of base metal tests involved investigation of varying minimum-to-maximum cyclic stress ratios. These tests made use of the same forging, specimen size, and maximum cyclic stress levels as used in the baseline test series. Test data for R values of 0.40 and 0.70 are included in Tables XI and XII, respectively. Results are plotted in Figures 18 and 19, respectively. It is noted that these results exhibit somewhat more scatter than observed in previous figures. This is felt to stem primarily from the fact that initial flaw sizes were quite difficult to measure. Texture of the initial flaw tends to blend with the texture of the area of cyclic growth. Thus, much of the apparent data scatter, especially at the highest R values and at the lowest stress intensity ratios, probably results from errors in flaw size measurement.

Weldment Cyclic Tests

Table XIII and Figure 20 contain the data applicable to cyclic tests performed on an Apollo tank weldment with flaws located in the heat affected zone. An average K_{Ic} value of 44.7 Ksi $\sqrt{\text{In}}$ was used in calculating stress intensity ratios.

In general, critical flaw sizes were not well defined. It does appear that in most if not all of the specimens cycled at a stress of 106 Ksi and lower, the flaw grew through the thickness prior to failure. This would be consistent with expected behavior only if increase in flaw depth occurred without a proportional increase in flaw length, 2c. For instance, for an a/2c value of about 0.35, calculated critical depth is slightly in excess of the thickness. Observation of the specimens cycled at 118 Ksi tends to confirm that this did happen. While the growth pattern in these specimens was impossible to measure accurately, it appears that most growth occurred in the depth direction. This is contrary to the usual behavior of the base metal specimens. Some increase in a/2c values occurred during cycling, but not to this extent. Regardless, the weldment data at the lower cyclic stress levels is of only limited value. Such data are marked with a "T" symbol in Figure 20.

5.0 DATA ANALYSIS

5.1 SUSTAINED LOAD BEHAVIOR

The results of the sustained load tests performed in the environment of N_2O_4 (Tables V and VI) are plotted in Figures 21 and 22 for test temperatures of 70° and 90°F, respectively. Data is plotted in terms of applied stress intensity against NO content. Data points reflect applicable forging, and increase, if any, in flaw growth during the sustained load period. Curves are drawn which reflect best estimates of the actual threshold values at the various NO levels tested. Results of Reference 1 testing are included for comparison. This includes an actual data point for the 70°F tests as shown in Figure 21, and an interpolated point for the 90°F test in Figure 22.

Two important conclusions can be drawn from the curves of Figures 21 and 22. First, threshold values increase steadily with increasing NO content through the range tested. This suggests that, in terms of vessel performance, an increase in the lower specification limit of NO content (presently set at 0.40 percent) would be desirable.

Secondly, it is observed that threshold ratios are relatively unaffected by rather large variations in actual toughness of different forgings. It is noted that the K_{Ic} values of the two forgings tested are 48.6 Ksi $\sqrt{\text{in}}$ for Fuel Cylinder #1 and 41.9 Ksi $\sqrt{\text{in}}$ for Fuel Cylinder #2; however, the threshold ratios appear to be quite similar.

5.2 CYCLIC FLAW GROWTH BEHAVIOR

5.2.1 Base Line Data

As noted in Section 4.4 a least square curve and a 99 percent confidence line were computed for all of the base line data and are shown in Figure 14. From observation of the actual data points of Figure 14 one might conclude that there is a stress level effect, and that lumping specimens of all stress levels may not be reasonable. Note that from these data, it appears that the greater cyclic lives tend to be associated with the higher cyclic stresses. This, of course is the opposite of expected behavior based upon growth rate laws which predict that cyclic growth rate is related primarily to the applied elastic stress intensity. That is:

$$\frac{da}{dN} = f(K_{max}, \Delta K)$$

Although successful correlations have been established for limited amounts of data using such laws, they have proved inadequate when compared to the broad

trend of cyclic crack growth data. Use of any of these laws, though would lead to a conclusion that highest cyclic stress at a given initial K level would result in the shortest cyclic life. This is not borne out in the data of Figure 14. Rather, it is felt that if any apparent stress dependence exists, it would be related to deep flaw effects. That is, for relatively low stresses, the flaws would grow deep with respect to thickness, and this extension would progress at a more accelerated rate than that of shallow flaws. This was briefly investigated as follows.

A cycles-to-failure curve was faired through the data points of the 0.100-inch thick AJG forging specimens cycled at a maximum cyclic stress of 126 Ksi. Final flaw sizes (critical size) for these specimens were apparently not very deep and were thus least affected by deep flaw magnification. This curve was differentiated to obtain growth rates. Next, a specimen (specimen K1-1c from Table VII) of the same forging, but cycled at 96 Ksi, was selected for comparison. This specimen failed in 136 cycles at an initial stress intensity ratio of 0.769. This ratio intersects the 126 Ksi curve at 320 cycles. By using initial flaw size in specimen K1-1c, and re-integrating the 126 Ksi rate curve (now accounting for changes in deep flaw effects) a predicted cyclic life of 276 cycles was calculated. This is only slightly less than that suggested by the high stress data points, and of course, still about twice the actual life of the specimen.

Based on the above, it is believed that stress level had little real influence on the data of Figure 14. All data points were thus used to develop the best fit least square curve shown. An additional point of $K_{Ii}/K_{Ic} = 1$ and $N = 1$ was also used. The curve was developed using a computer program (DATAN), which isolates and analyzes the prominent geometric characteristics of the data and prescribes an appropriate fitting function with similar geometric characteristics. It fits the least square curves of various degrees of polynomials and rational functions if the data is asymptotic. It then chooses the one which has the least error. The best fit least square curve for the data is represented by the following equation:

$$K_{Ii}/K_{Ic} = A + B \log_{10} N + C(\log_{10} N)^2$$

where $A = 0.99976$, $B = 0.01942$, $C = 0.04996$

Since the ratio of stress intensities, K_{Ii}/K_{Ic} contains errors due to measurements of flaw sizes, stress levels, etc., K_{Ii}/K_{Ic} is taken as dependent variable and N as an independent variable in the above fit.

Utilizing the above least square curve and data points, standard error of estimate for K_{Ii}/K_{Ic} is established which is 0.02267.

Examining the scatter of data points with comparison to the least square curve very carefully in Figure 14, it is concluded that the variance of K_{Ii}/K_{Ic} is nearly constant in the range of data, i.e., N equal or greater than 40. It is also known that for any degree of confidence band, the curve has to pass through the point N = 1 and $K_{Ii}/K_{Ic} = 1$. Hence the variance of K_{Ii}/K_{Ic} at $K_{Ii}/K_{Ic} = 1$ and N = 1 is zero. It is then assumed that the variance of K_{Ii}/K_{Ic} varies linearly between N = 1 and N = 40 and for $N \geq 40$ it has the constant value as established from the data and the least square curve. Based on these assumptions and using the student's t - distribution table for 43 (46-3) degrees of freedom, 99.1 confidence band is established which is shown in Figure 14. Differentiating the least square curve and the 99% confidence curve gives the growth rate curves of Figure 23.

5.2.2 Heat-to-Heat Variation

While it was the original intent to provide a direct comparison of the effect on cyclic behavior of different forgings, unfortunately, available raw material was thinner than desired, and the tests were complicated by this second variable. The series of reduced thickness AJG forging tests were thus programmed. The results of these tests along with the two other thin forgings are all plotted in Figure 24. For comparison, the upper and lower bound curves of the base line data is included in the figure. While the thin specimen data generally falls to the left of the base line data, significantly there is no noticeable difference between the three sets of thin specimens. To determine the cause of the reduced cyclic life of the thin specimens, an excercise similar to that noted earlier was performed. Specimen GI-13A (See Table X), an AJG reduced thickness specimen was selected. This specimen was selected because both initial and critical flaw sizes were relatively well defined. This specimen failed in 397 cycles at an initial stress intensity ratio of 0.666. Initial and critical flaw depth, a, and length, 2c, were 0.0272 x 0.131, and 0.0460 x 0.165-inches, respectively. It was assumed that flaw shape changes (a/2c values) progressed in a linear manner from initial-to-critical. Using the least square rate data, and accounting for deep flaw effects, it was predicted that the cyclic life of this specimen was 412 cycles. (Sample calculations are shown in Table XIV) Note that the stress intensity ratio of 0.666 line intersects the thick specimen curve at about 630 cycles.

From the above, it is concluded that the apparent differences between the cyclic behavior of the Apollo forgings and the AJG forgings stem almost entirely from specimen dimension variables, and do not represent a significant raw material variable.

5.2.3 The Effect of Varying R Values

In Figures 18 and 19, nominal curves were drawn thru the data points of the

specimens tested at R = 0.40 and R = 0.70. The curves represent a fixed percentage, at each K level, to the right of the least square curve generated from the base line data (i.e., the R = 0.10 data). Actual relative lives are 1.68 and 18.1 times the base line lives for the R = 0.40 and R = 0.70 data, respectively. For purposes of comparison, these numbers were compared with values predicted by several growth rate laws. These included an estimate by Roberts and Erdogan (Ref. 2):

$$\text{relative } \frac{da}{dN} = f\left[(1+\beta)^2 (\Delta K)^4\right]$$

$$\text{where } \beta = \frac{K_{max} + K_{min}}{2\,\Delta K}$$

an estimate by Krafft (Ref. 3):

$$\text{relative } \frac{da}{dN} = f(\gamma)$$

$$\text{where } \gamma = \frac{K_{max} - K_{min}}{K_{max}} \;\&\; f(\gamma) = \left[1 - (1-\gamma)^2\right]\left[1+\gamma\right]^4$$

and an estimate by Forman (Ref. 4):

$$\text{relative } \frac{da}{dN} = \frac{(\Delta K)^n}{(1-R)K_{Ic} - \Delta K}$$

A comparison of these results is made in Figure 25. It is noted that all of the above laws tend to over estimate cyclic life at low R values and under estimate the life at high R values, when compared to the experimental data.

For purposes of analyzing 6Al-4V STA vessels, it is recommended that the experimentally derived curve shown in Figure 25 be used.

5.2.4 Weldment Data

Figure 20 showed weldment HA7 cyclic data and compared that data with the base line base metal least square curve. The weldment cyclic lives are in all cases above the base metal curve. It was observed that fracture faces of these specimens exhibited very coarse texture and flaw peripheries were quite jagged when viewed from the direction of crack propagation. Presumably these irregularities attributed to the higher apparent cyclic lives of these specimens, because the apparent critical toughness values would probably be elevated. In

effect this would result in an effective initial stress intensity ratio lower than calculated. Since microstructure can vary markedly throughout the heat affected zone, cyclic behavior would also be expected to vary. It is therefore considered that these higher values should not be used in vessel analysis: it is presently recommended that the base metal growth rates be used for both base metal, and weld metal analyses.

6.0 CONCLUSIONS & RECOMMENDATIONS

1. Results of sustained load tests of 6Al-4V forgings in the environment of nitrogen tetroxide show that;

   a) Threshold ratios increase steadily with increasing NO content. In terms of vessel performance, this suggests that an increase in the lower specification limit (presently set at 0.40 percent NO) would be desirable.

   b) Threshold ratios are relatively unaffected by rather wide variations in actual K_{Ic} values.

2. Results of the cyclic tests show that;

   a) Of the three forging heats tested, heat-to-heat variations in cyclic behavior are insignificant.

   b) When compared with the experimental results, existing growth rate laws over estimate cyclic life at low R values and under estimate cyclic life at high R values.

   c) Cyclic life of specimens flawed in the weld heat affected zone appear to be higher than that of base metal. However, since microstructure (and presumably, fracture characteristics) can vary markedly throughout the heat affected zone, it is presently recommended that the base metal growth rates be used for both base metal and weldment analysis.

REFERENCES

1. Tiffany, C. F., and Masters, J. N., "The Flaw Growth Characteristics of 6Al-4V Titanium Used in Apollo Spacecraft Pressure Vessels", NASA CR-65586, March, 1967.

2. Roberts R., and Erdogan, R., "The Effect of Mean Stress on Fatigue Crack Propagation in Plates Under Extension and Bending", ASME Paper No. 67, WA/Met-2, 1967.

3. Krafft, J. M., "A Comparison of Cyclic Fatigue Crack Propagation with Single Cycle Crack Toughness and Plastic Flaw", Report to ASTM Fracture Toughness of High Strength Materials Special Committee, September 1964.

4. Foreman, R. G., Kearney, V. E., and Engle, R. M., "Numerical Analysis of Crack Propagation in Cyclic Loaded Structures", ASML Paper No. 66-WA/Met-4, 1967.

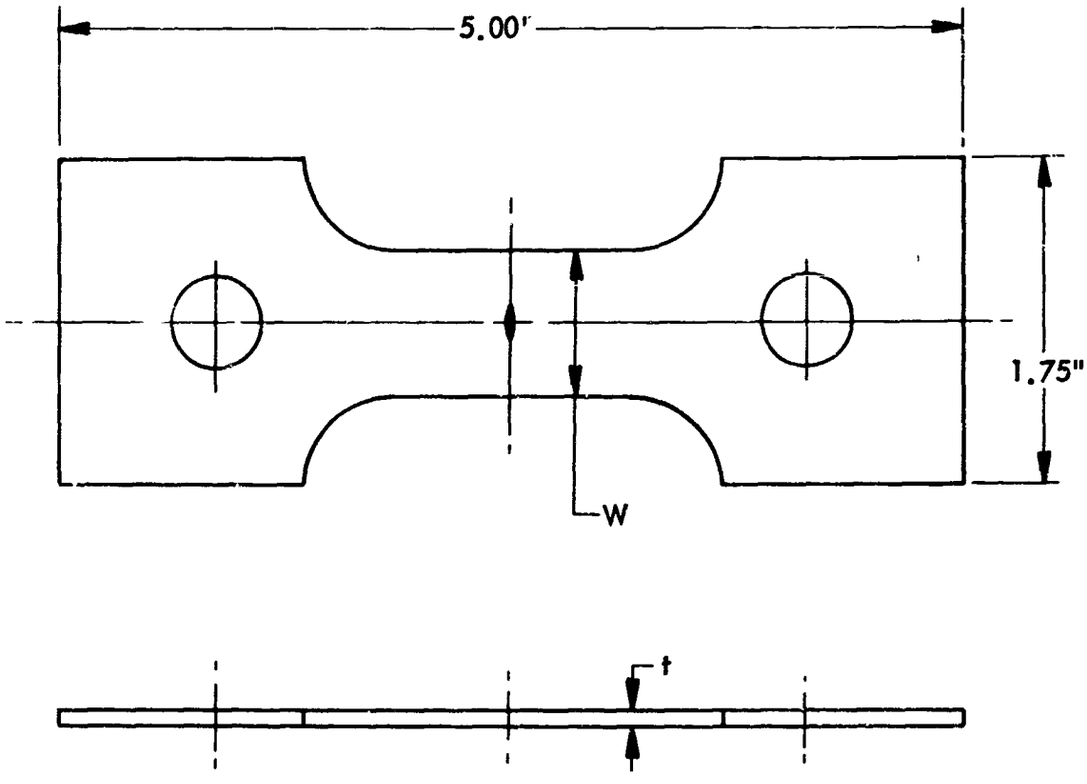

Figure 1 : AEROJET GENERAL FORGING SPECIMEN CONFIGURATION

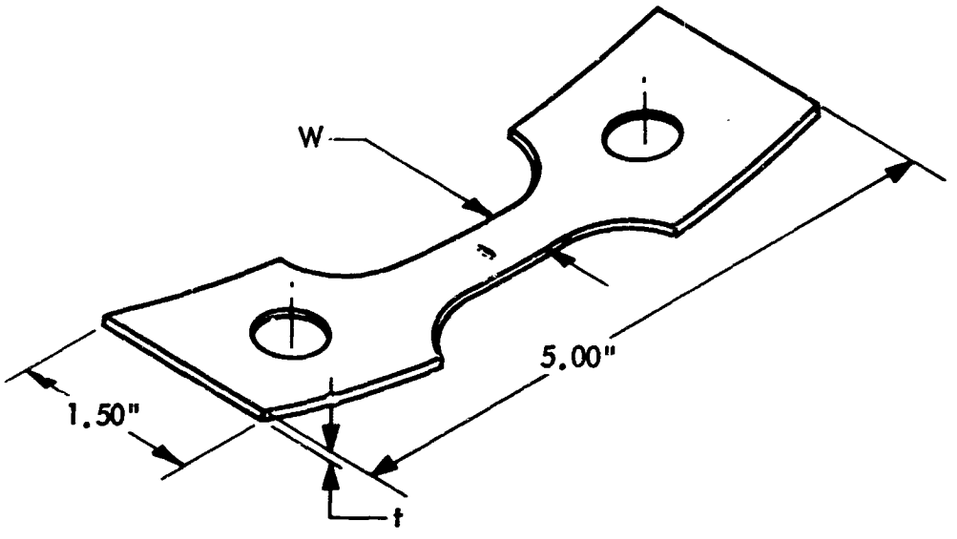

a) "L" SPECIMENS

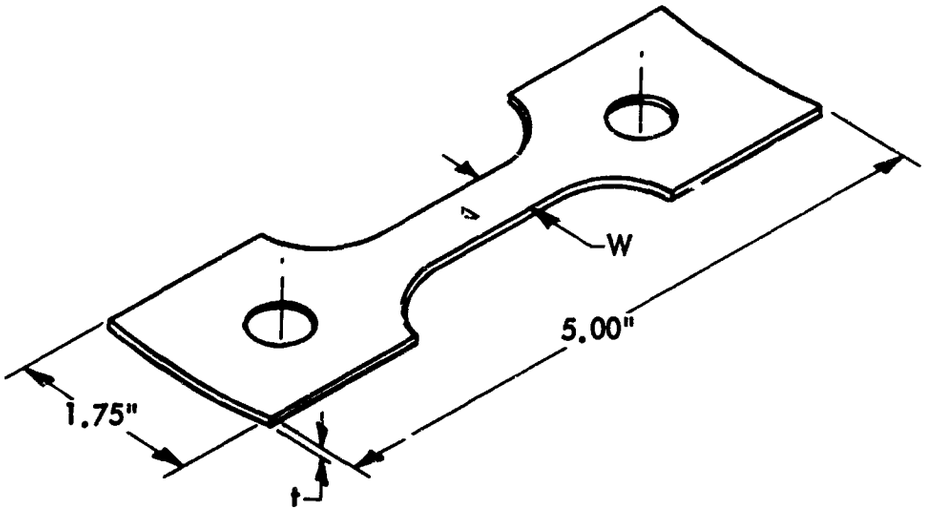

b) "T" SPECIMENS

Figure 2 : APOLLO TANK CYLINDER SPECIMEN CONFIGURATIONS

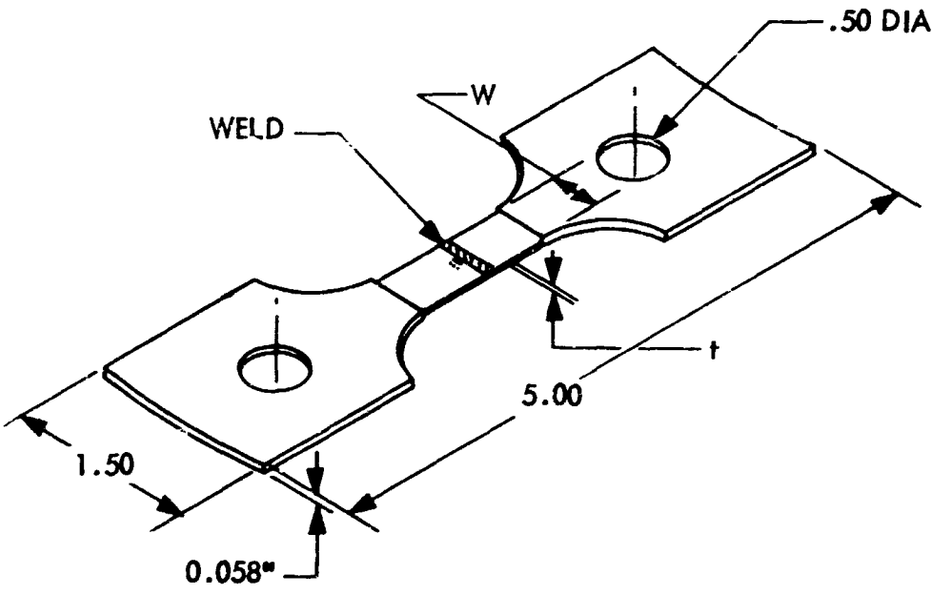

Figure 3: WELD SPECIMEN CONFIGURATION

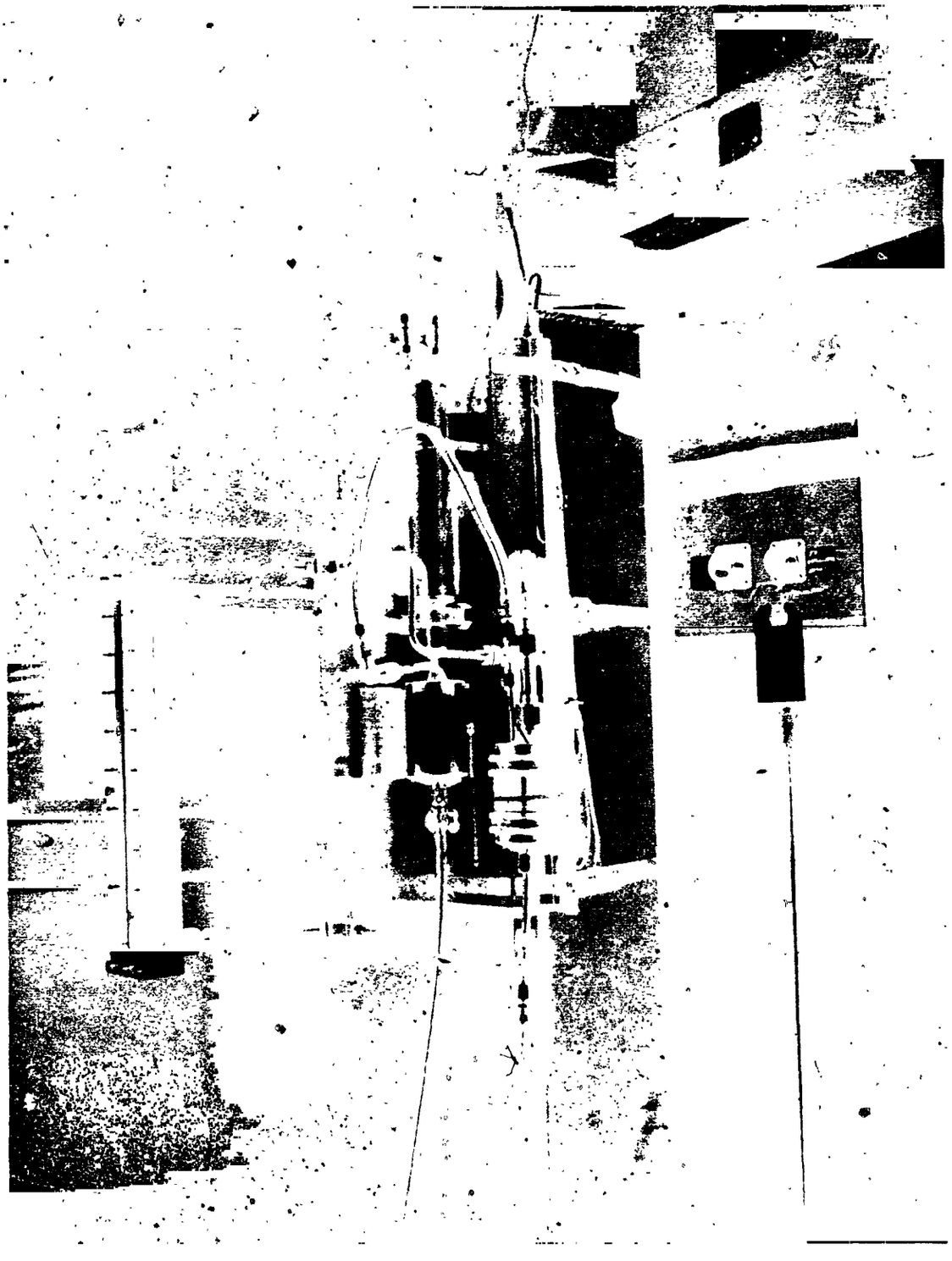

Figure 4: SUSTAINED LOAD TEST SETUP SHOWING N_2O_4 SUPPLY SYSTEM

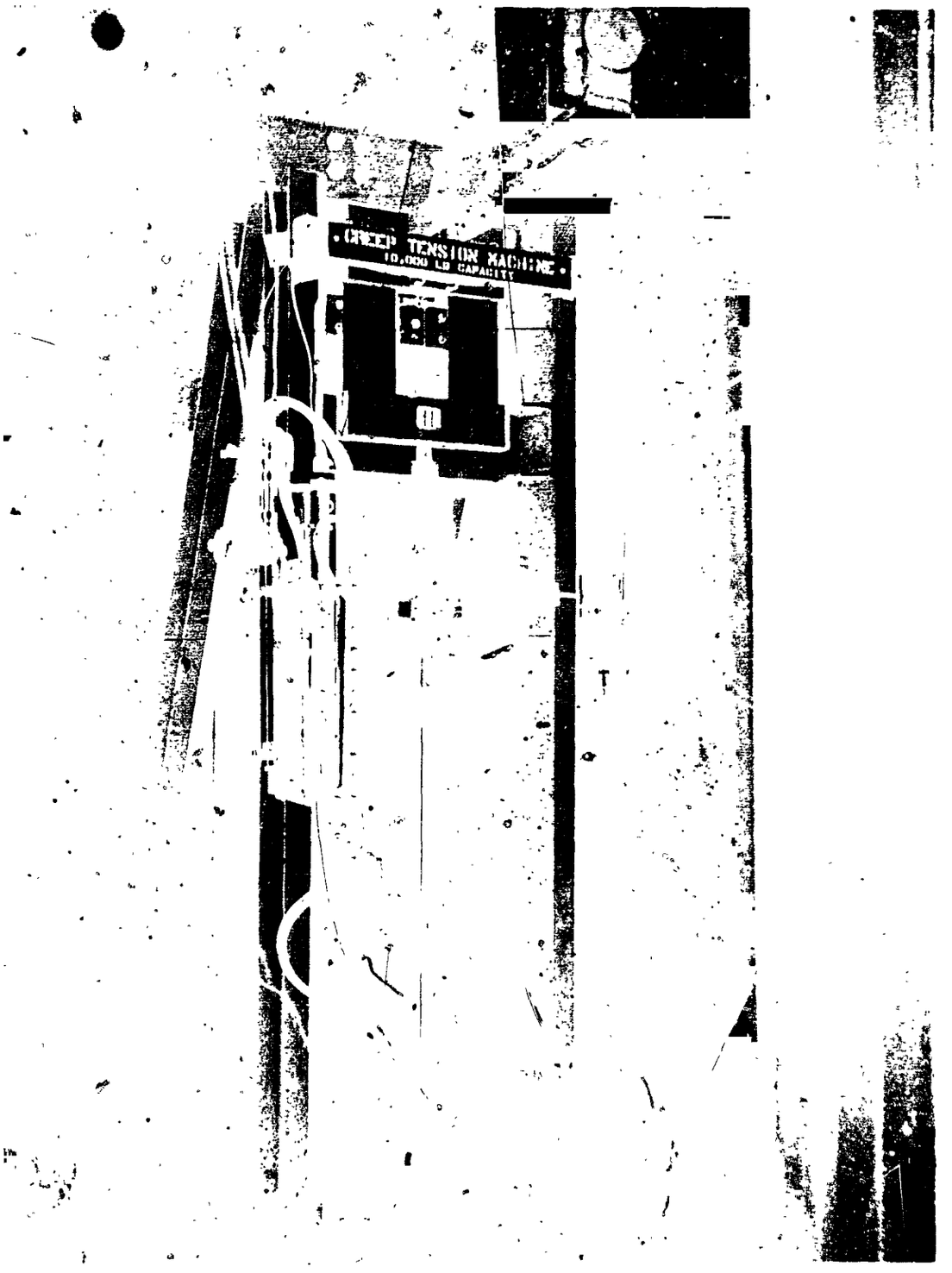

Figure 5: SUSTAINED LOAD TEST SETUP - OVERALL VIEW

Figure 6: SUSTAINED LOAD TEST SETUP SHOWING SPECIMEN MOUNTING DETAIL

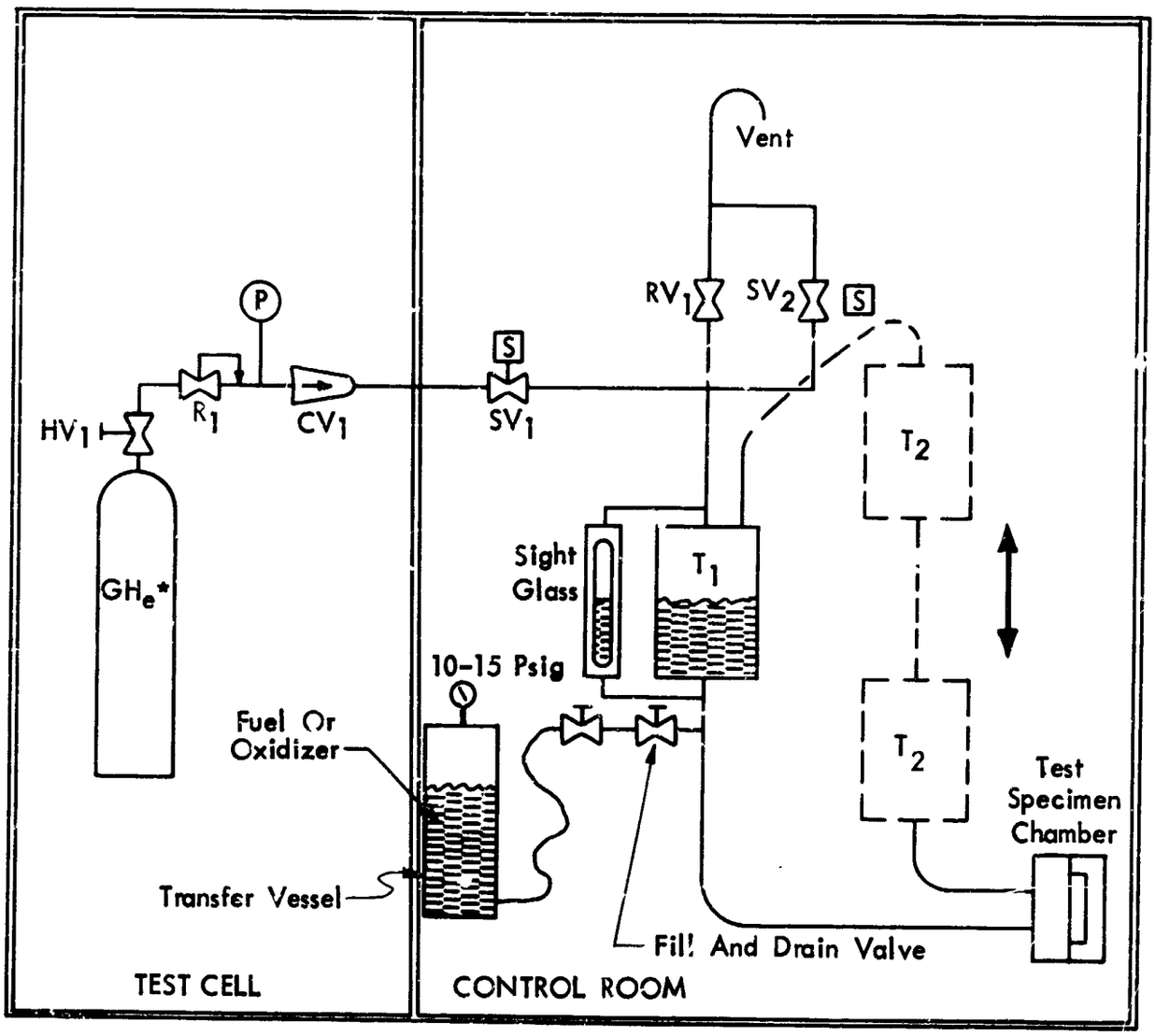

T_1 = Circulating Tank - Stationary

T_2 = Circulating Tank - Cycling

SV_1 = Normally Closed Solinoid Valve, 115 Vac

SV_2 = Normally Open Solinoid Valve, 115 Vac (Vent Valve)

RV_1 = Relief Valve, 280 Psig

CV_1 = Check Valve, 300 Psi

* H_e System Also Used For Purging System

Figure 7 : FLUID AND PRESSURIZATION SYSTEM SCHEMATIC

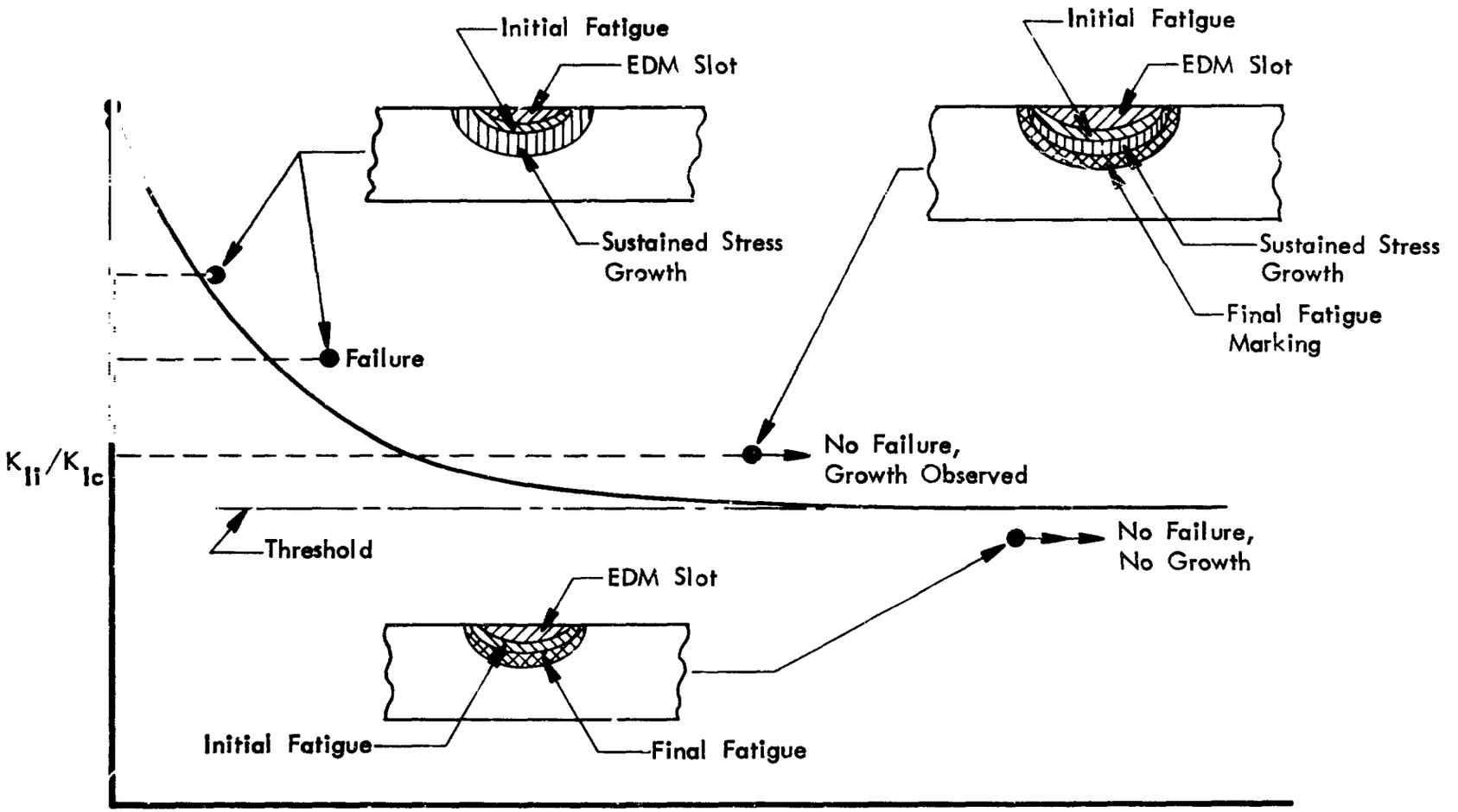

Figure 8 : SUSTAINED STRESS FLAW GROWTH TEST APPROACH

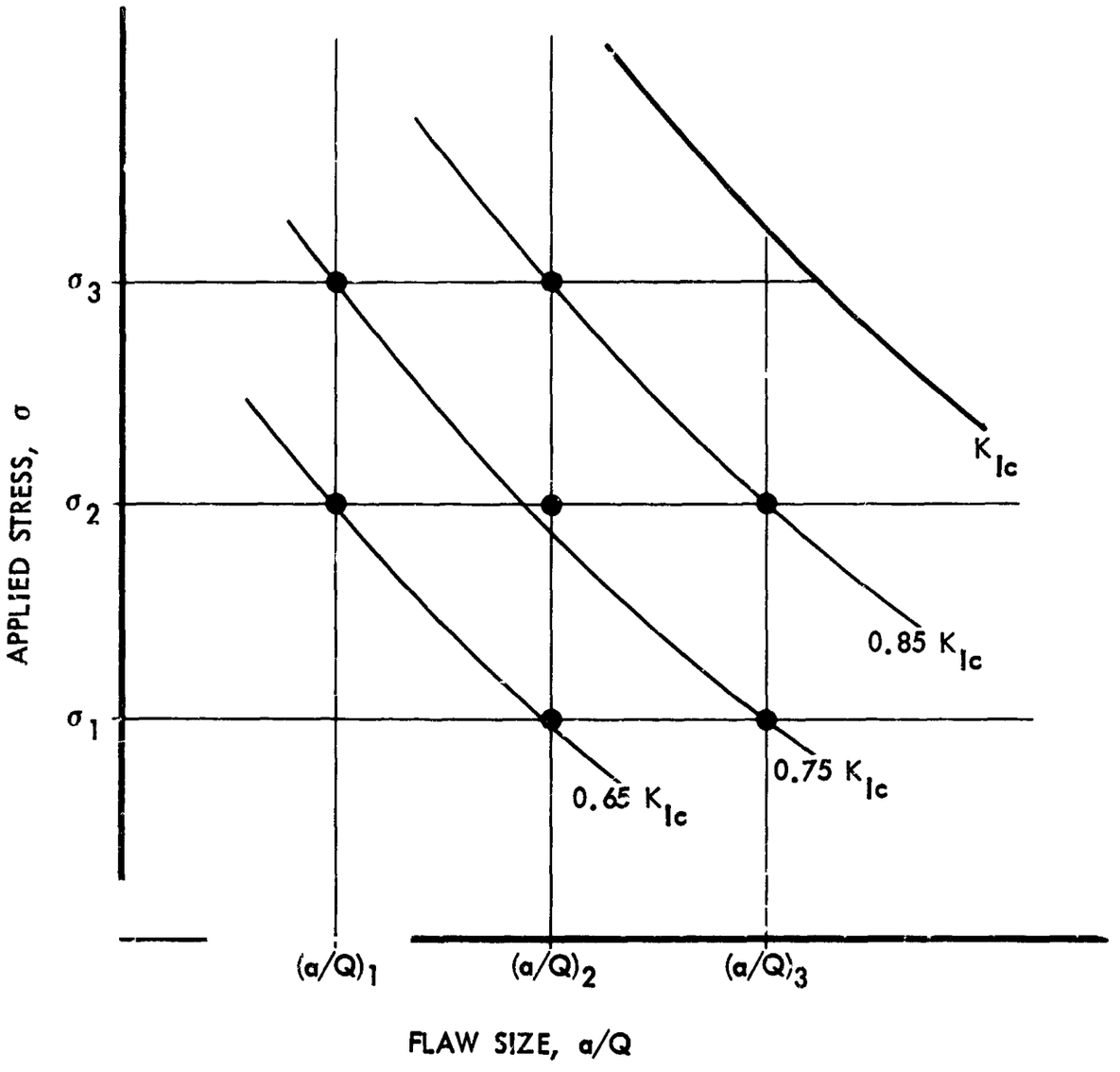

Figure 9 : SCHEMATIC OF CYCLIC TEST PROGRAMMING PROCEDURES

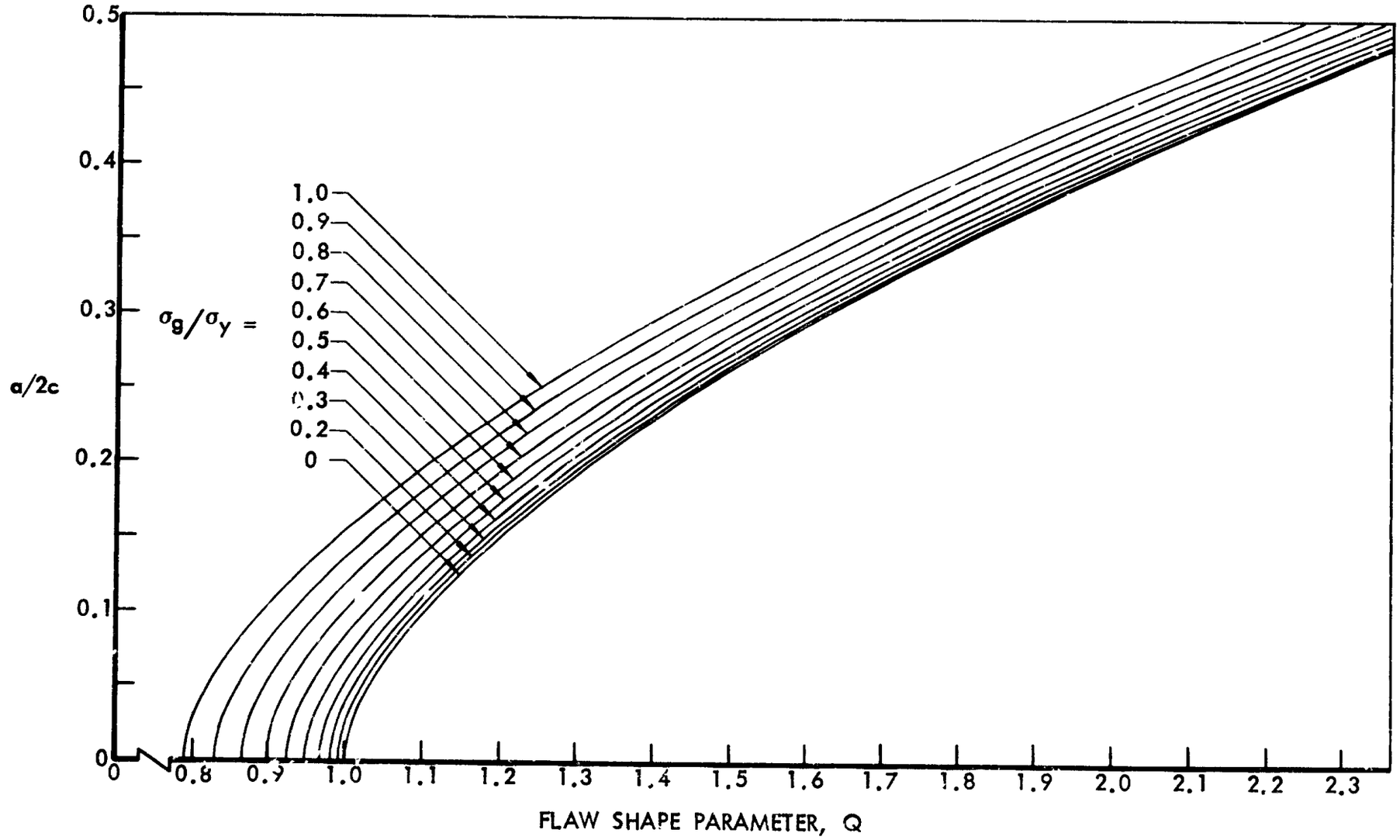

Figure 10: SHAPE PARAMETER CURVES FOR SURFACE AND INTERNAL FLAWS

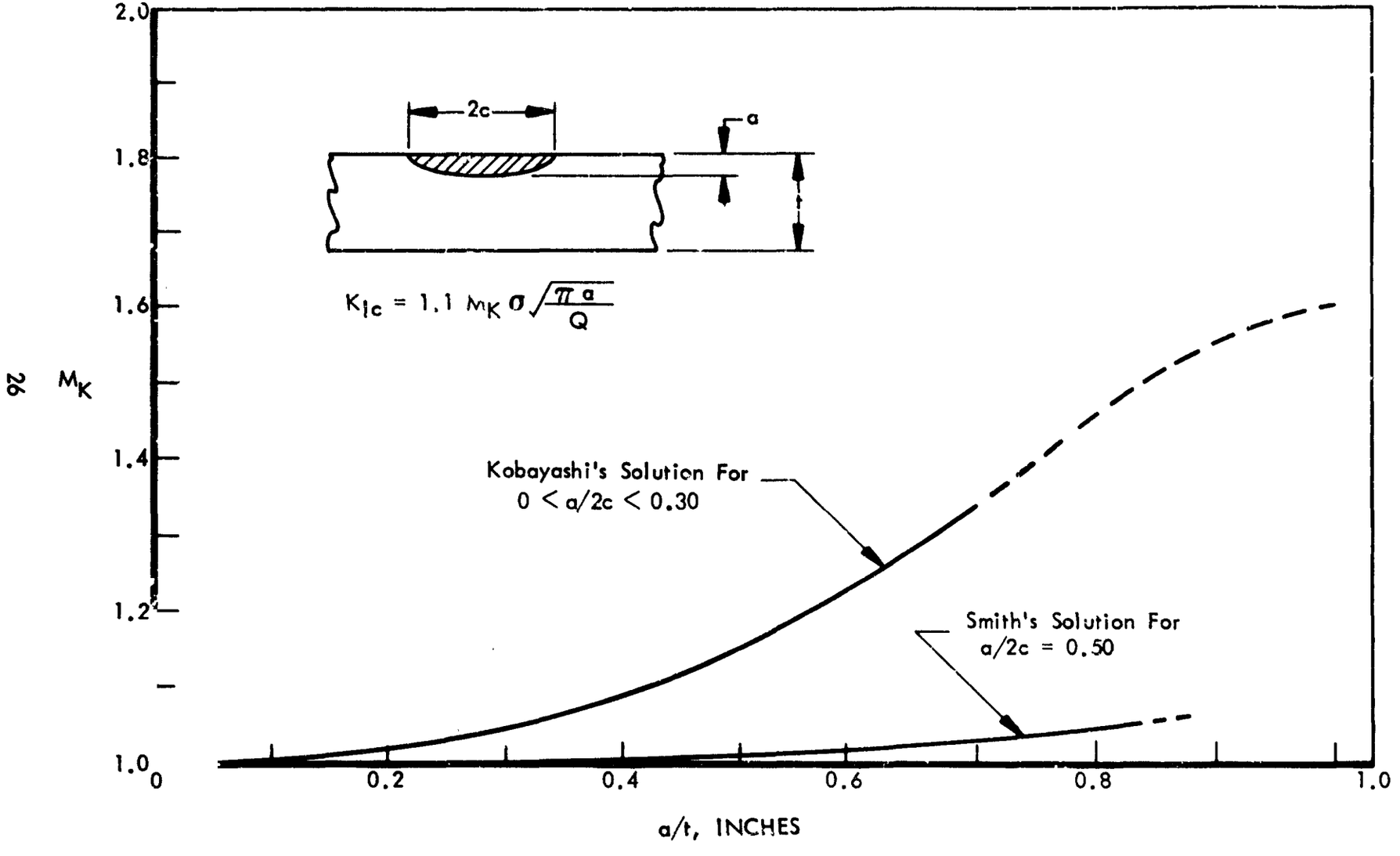

Figure 11: STRESS INTENSITY MAGNIFICATION FACTORS FOR DEEP SURFACE FLAWS

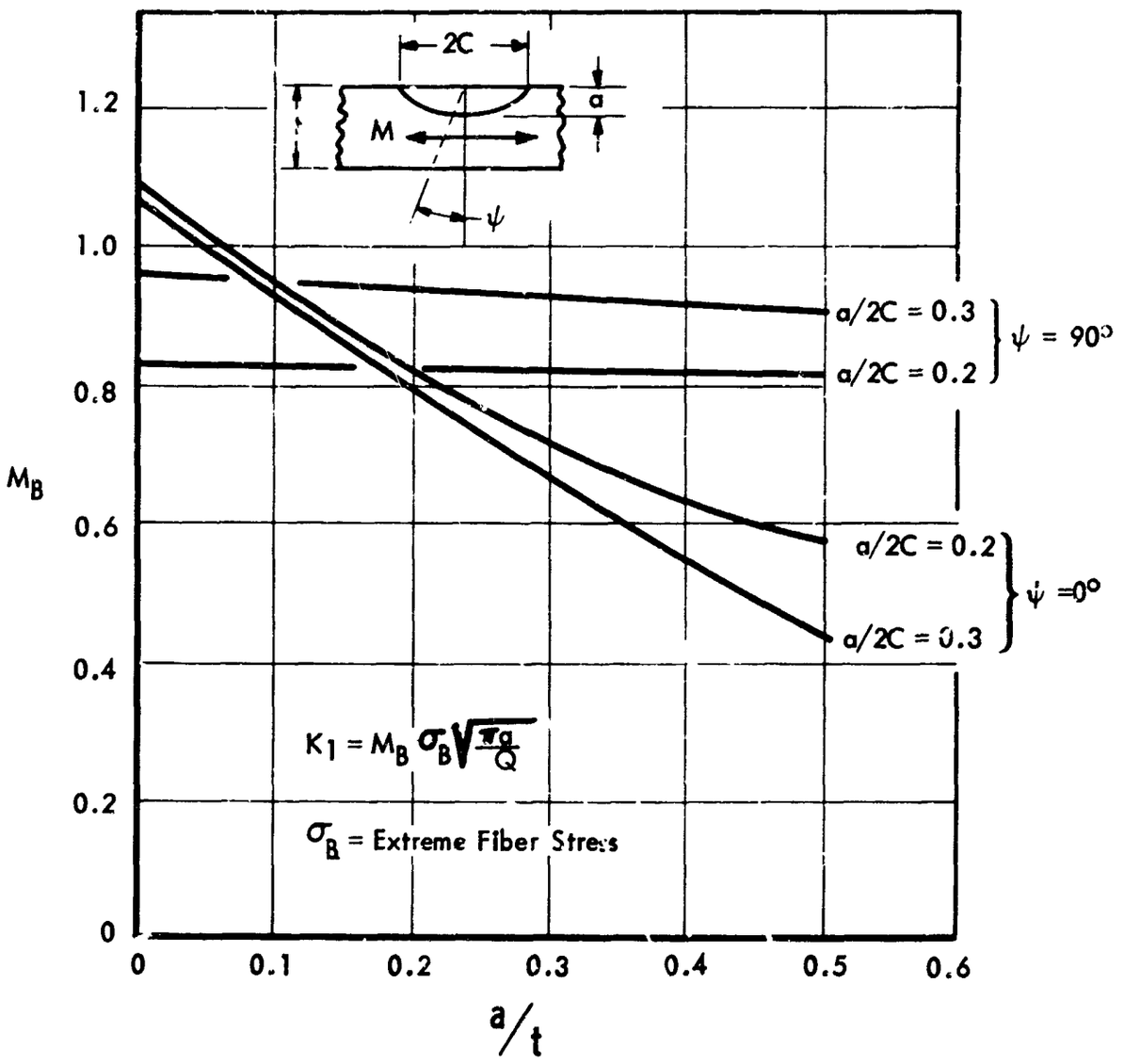

Figure 12: APPROXIMATE STRESS INTENSITY FACTORS FOR SURFACE FLAWS IN BENDING

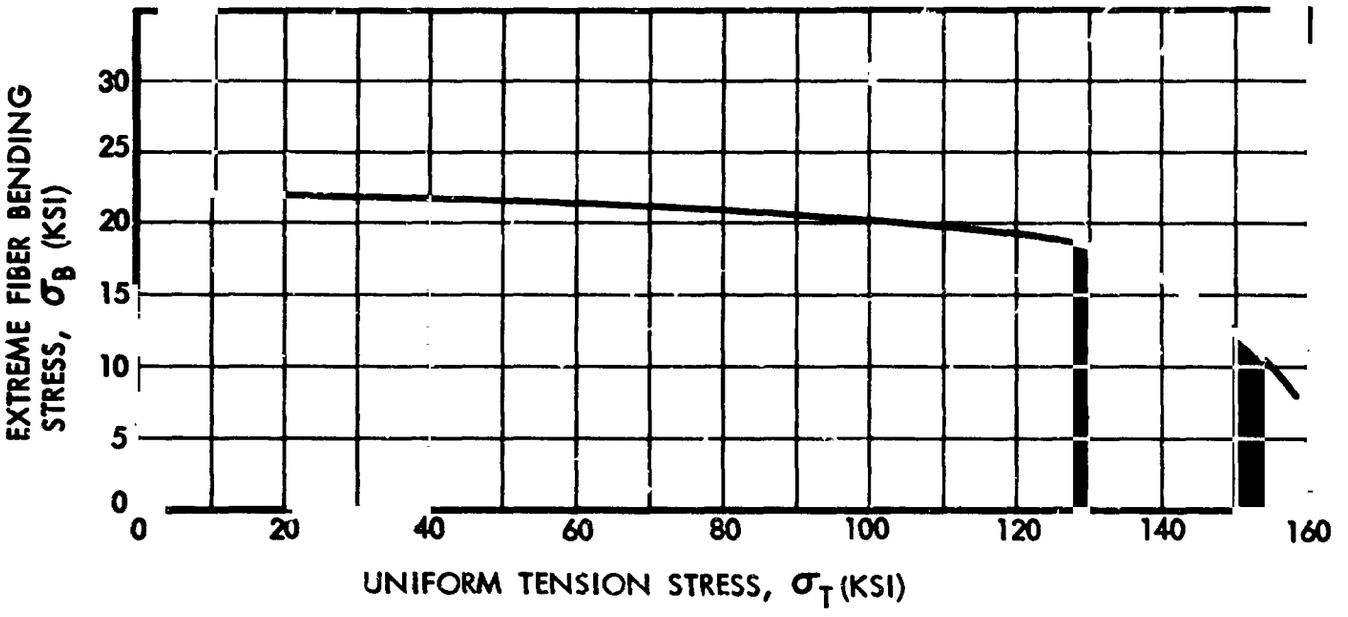

Figure 13: BENDING STRESS IN CURVED SPECIMENS

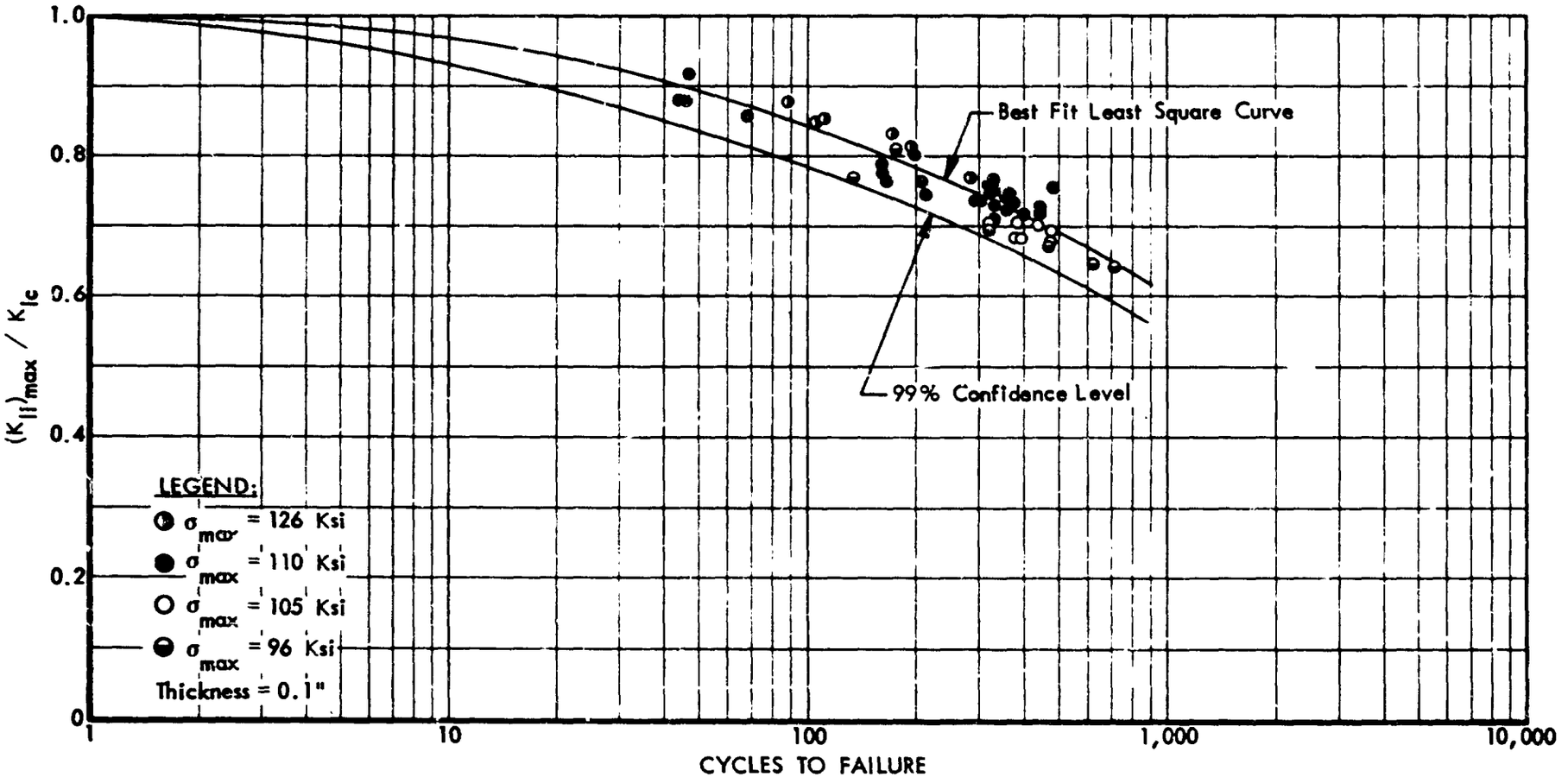

Figure 14: CYCLIC FLAW GROWTH CURVE FOR AEROJET GENERAL FORGING
R = 0.10 ENVIRONMENT = R.T. AIR

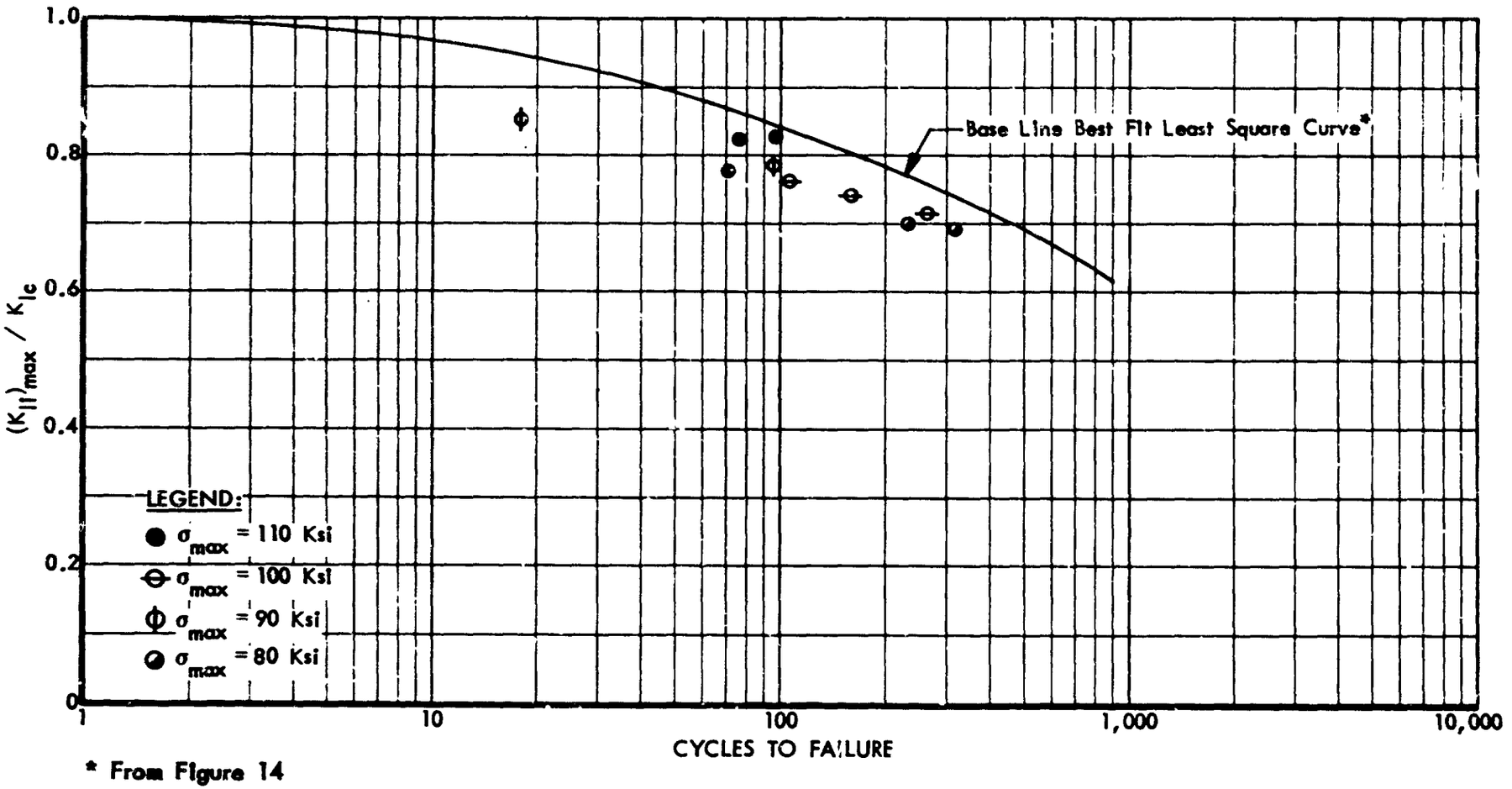

* From Figure 14

Figure 15: CYCLIC FLAW GROWTH CURVE FOR APOLLO FUEL CYLINDER #2
R = 0.10 ENVIRONMENT = R.T. AIR

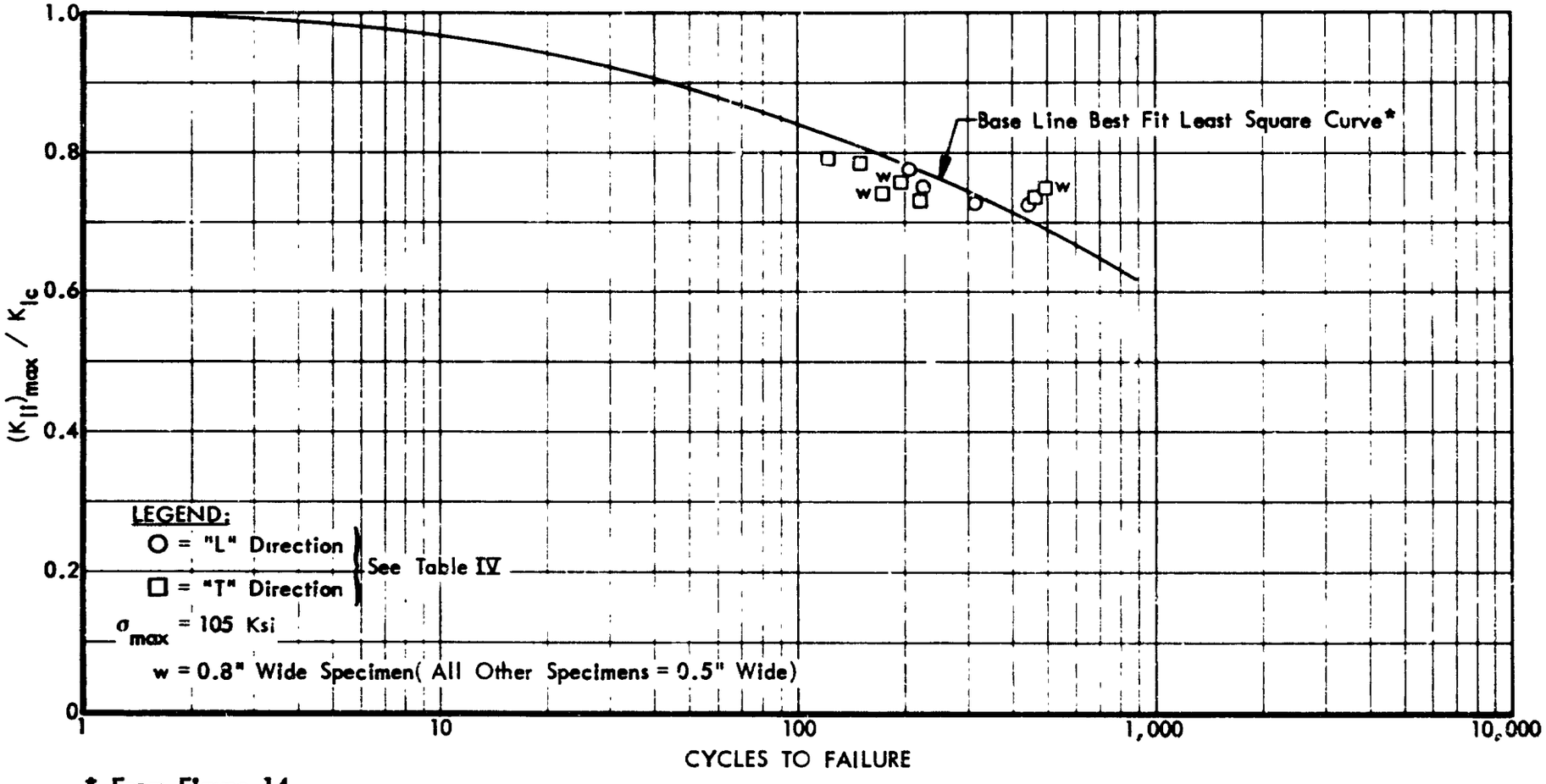

* From Figure 14

Figure 16: CYCLIC FLAW GROWTH CURVE FOR APOLLO OXIDIZER CYLINDER #1

R = 0.10 ENVIRONMENT = R.T. AIR

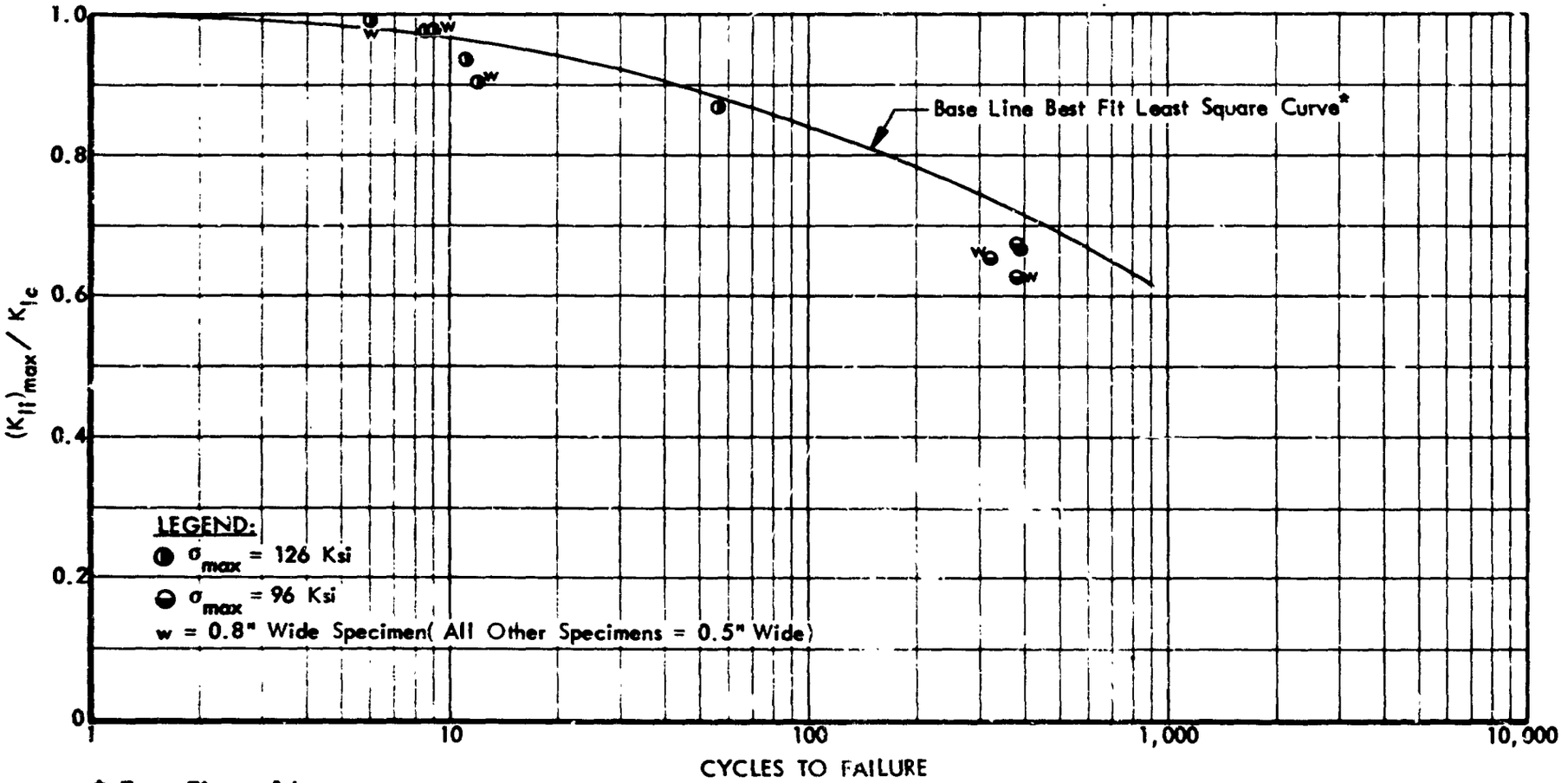

* From Figure 14

Figure 17: CYCLIC FLAW GROWTH CURVE FOR AEROJET GENERAL FORGING
(Reduced Thickness)

R = 0.10 ENVIRONMENT = R.T. AIR

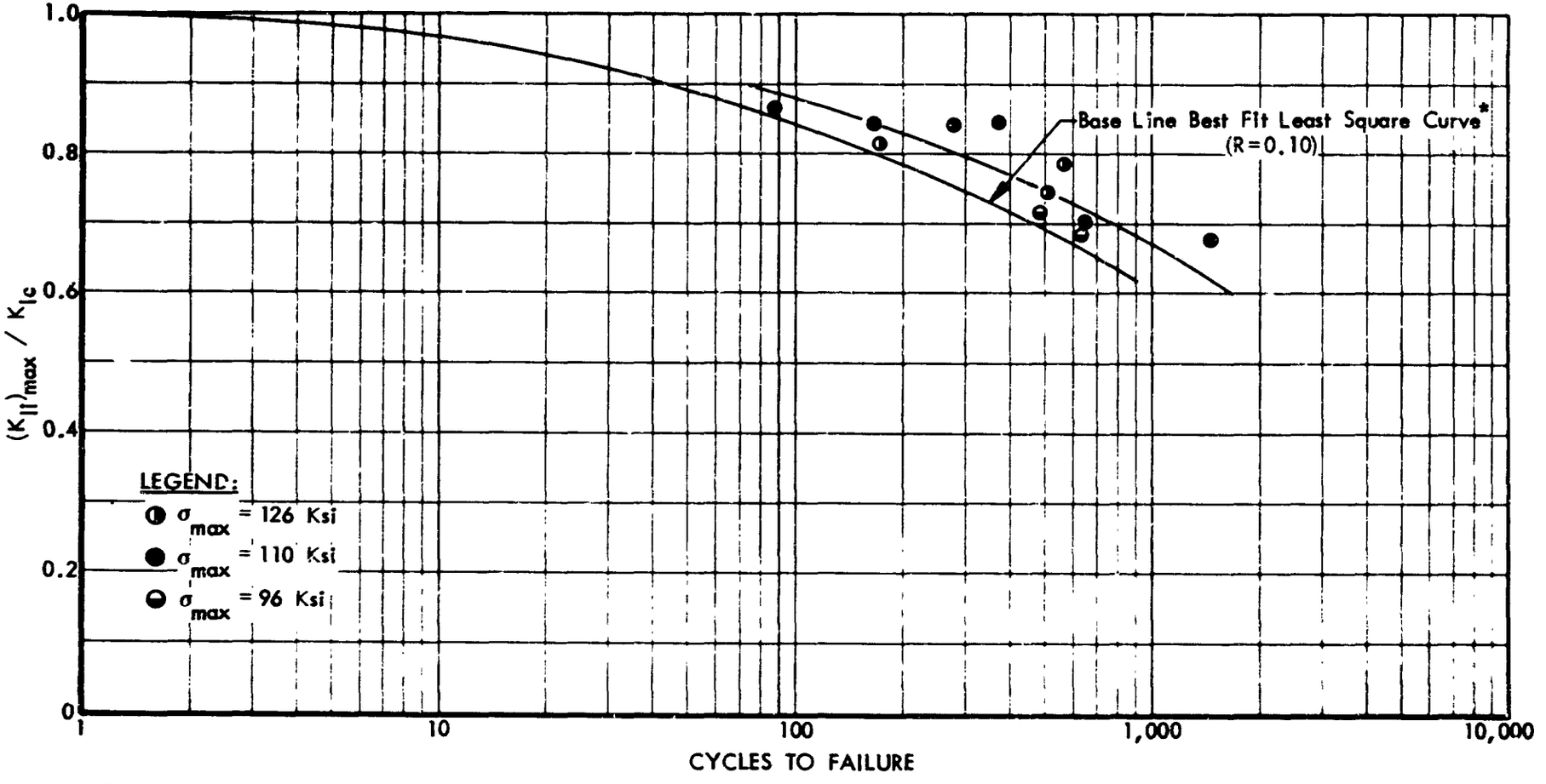

* From Figure 14

Figure 18: CYCLIC FLAW GROWTH CURVE FOR AEROJET GENERAL FORGING
R = 0.40 ENVIRONMENT = R.T. AIR

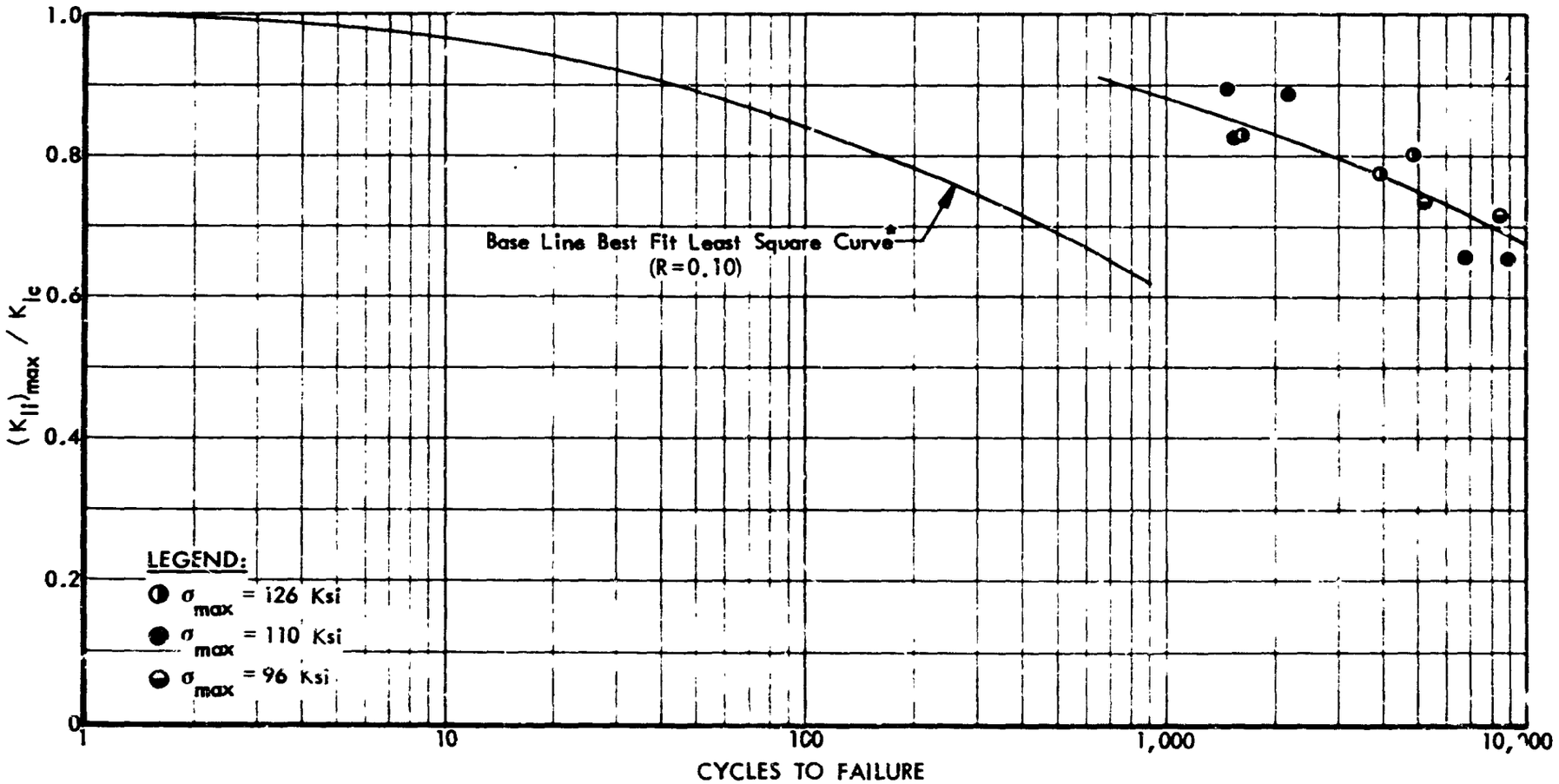

* From Figure 14

Figure 19: CYCLIC FLAW GROWTH CURVE FOR AEROJET GENERAL FORGING

R = 0.70 ENVIRONMENT = R.T. AIR

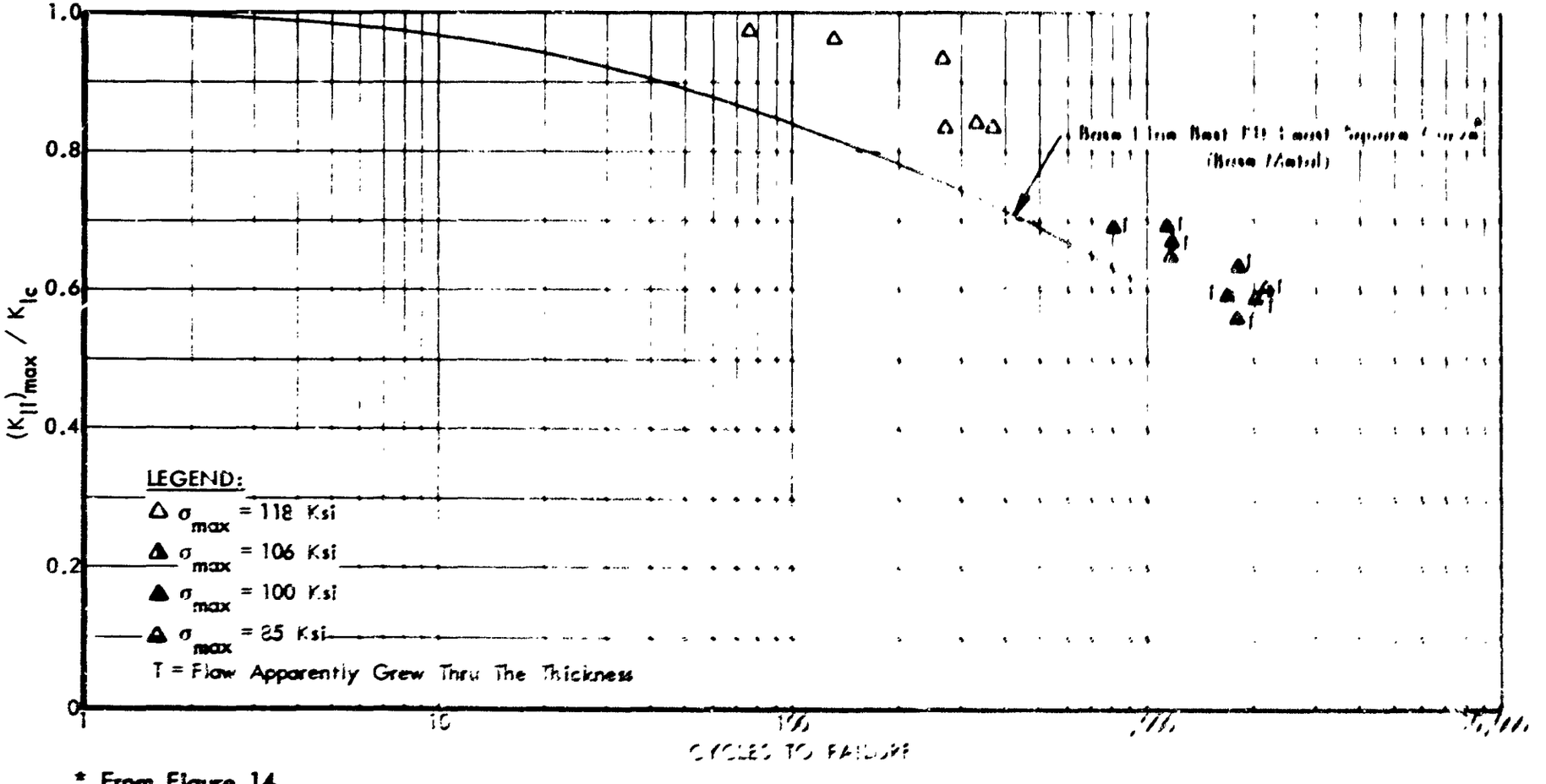

* From Figure 14

Figure 20: CYCLIC FLAW GROWTH CURVE FOR APOLLO TANK MATERIAL
R = 0.10 ENVIRONMENT - [illegible]

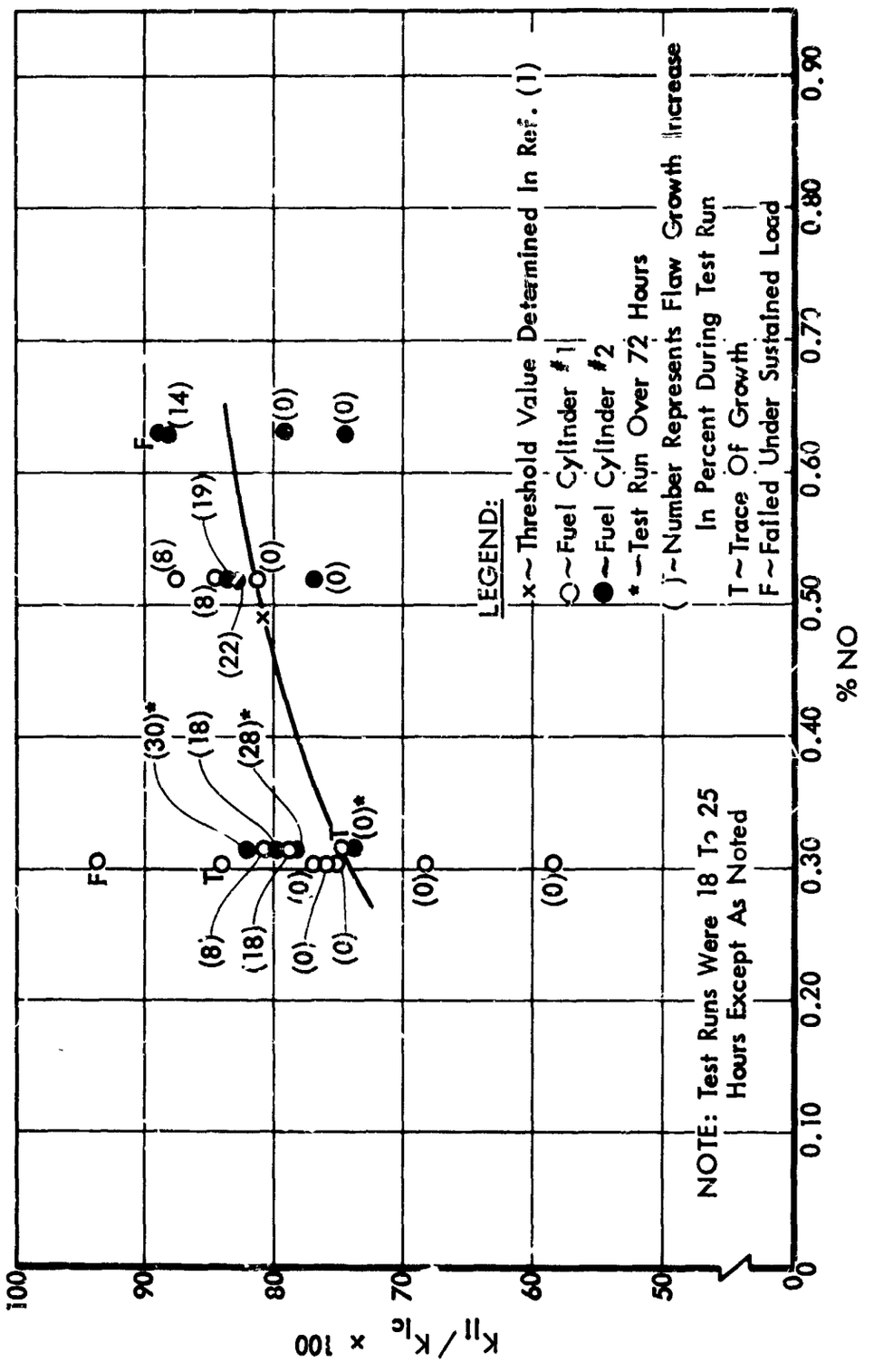

Figure 21: EFFECT OF NITRIC OXIDE CONTENT ON K_{TH} (70 °F Test Temperature)

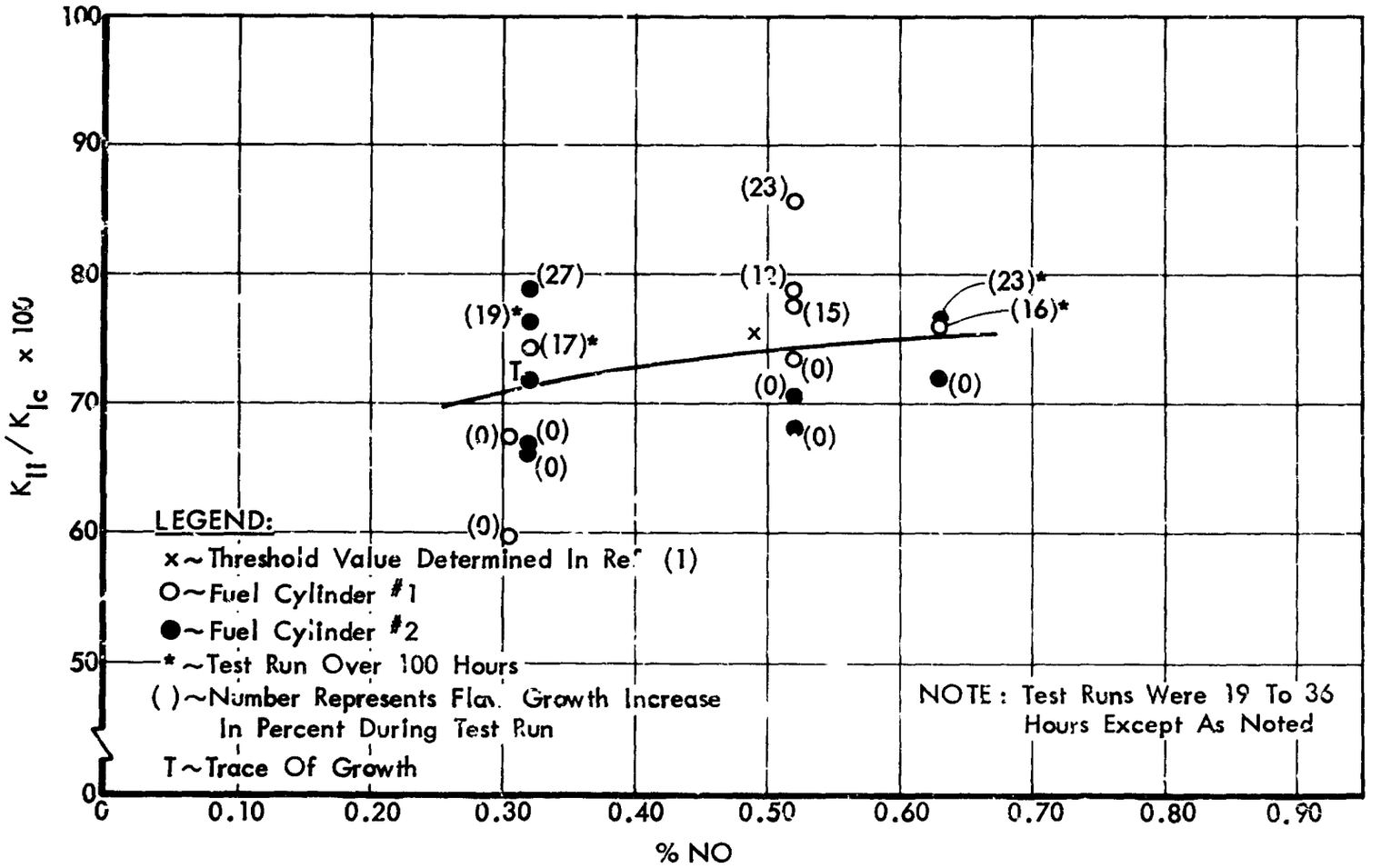

Figure 22: EFFECT OF NITRIC OXIDE CONTENT ON K_{TH} (90 °F Test Temperature)

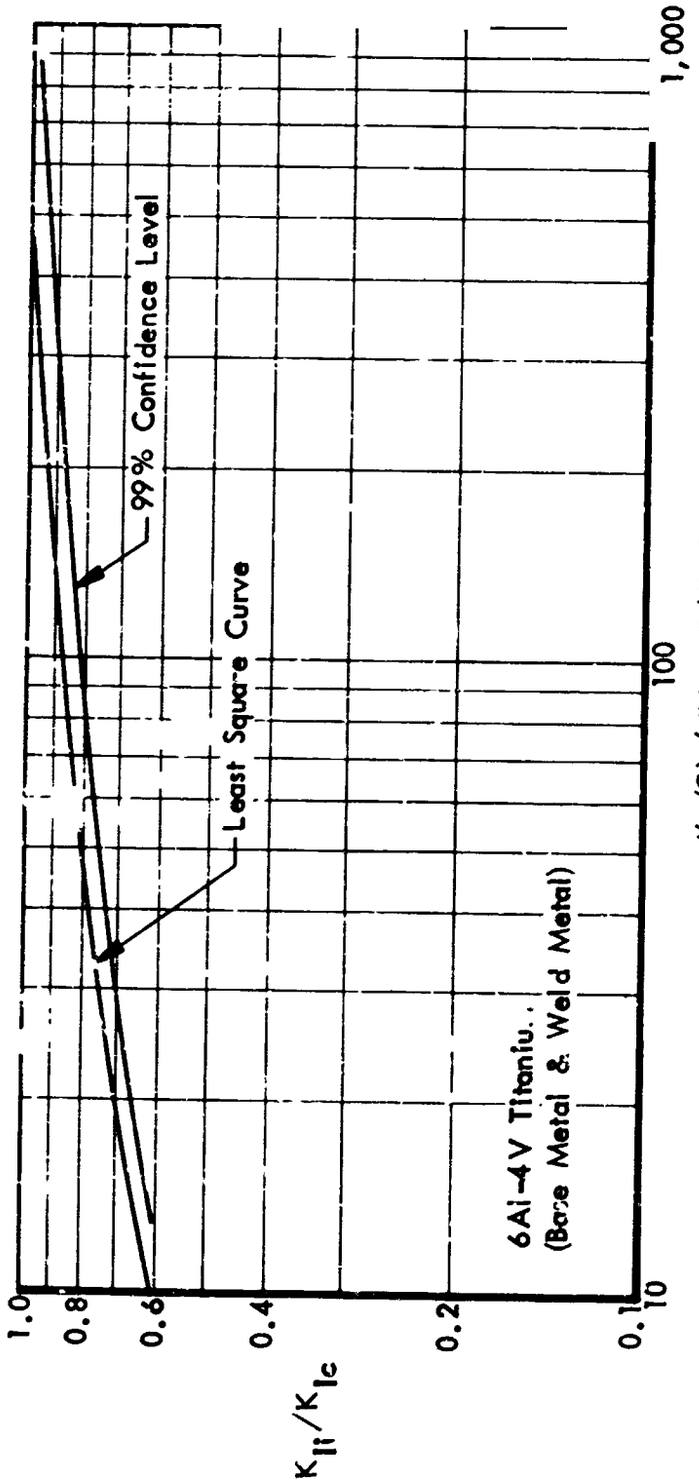

Figure 23: CYCLIC FLAW GROWTH RATES (For σ_{max} = 100 Ksi)

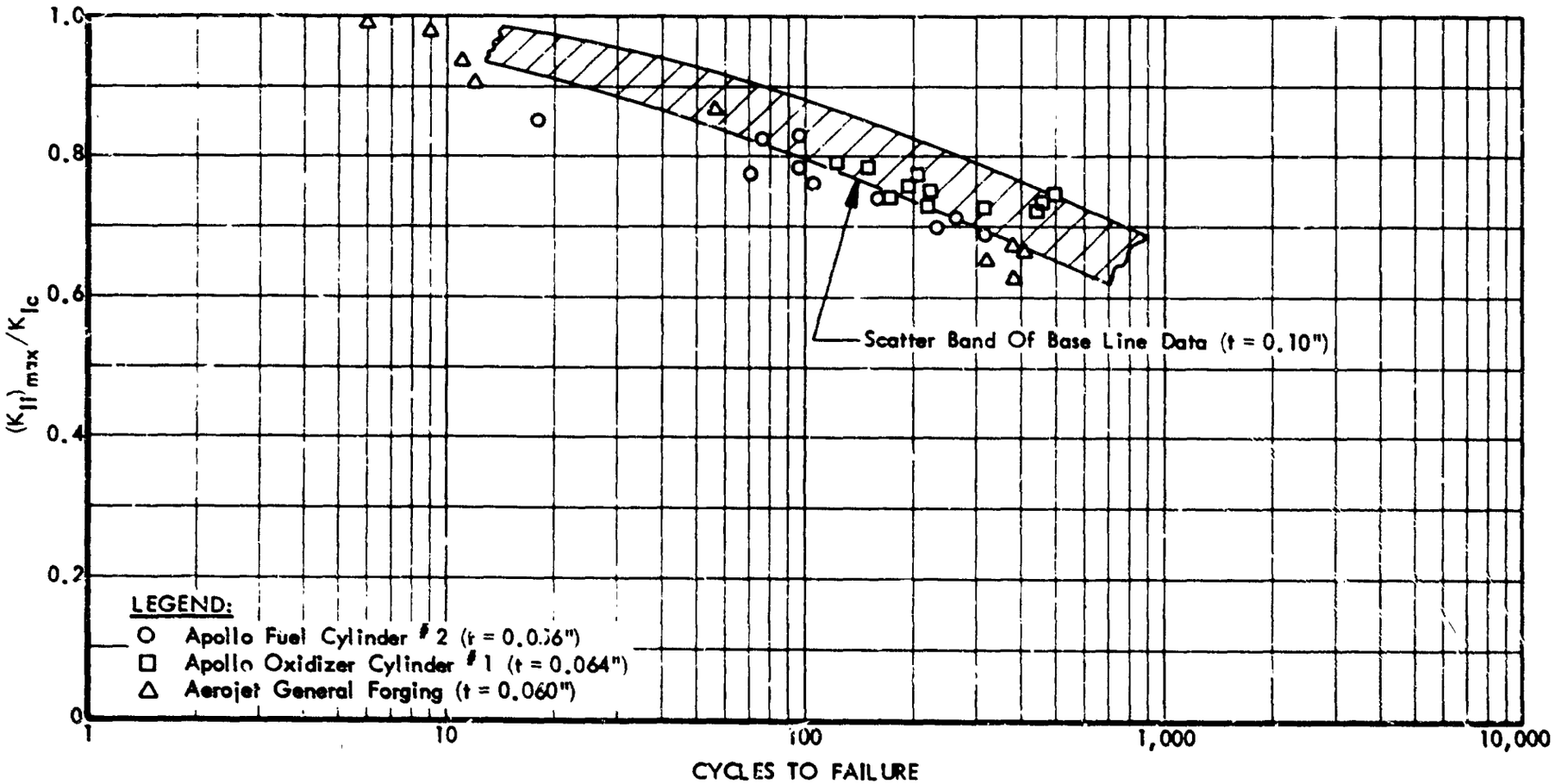

Figure 24: EFFECT OF SPECIMEN THICKNESS ON CYCLIC LIFE

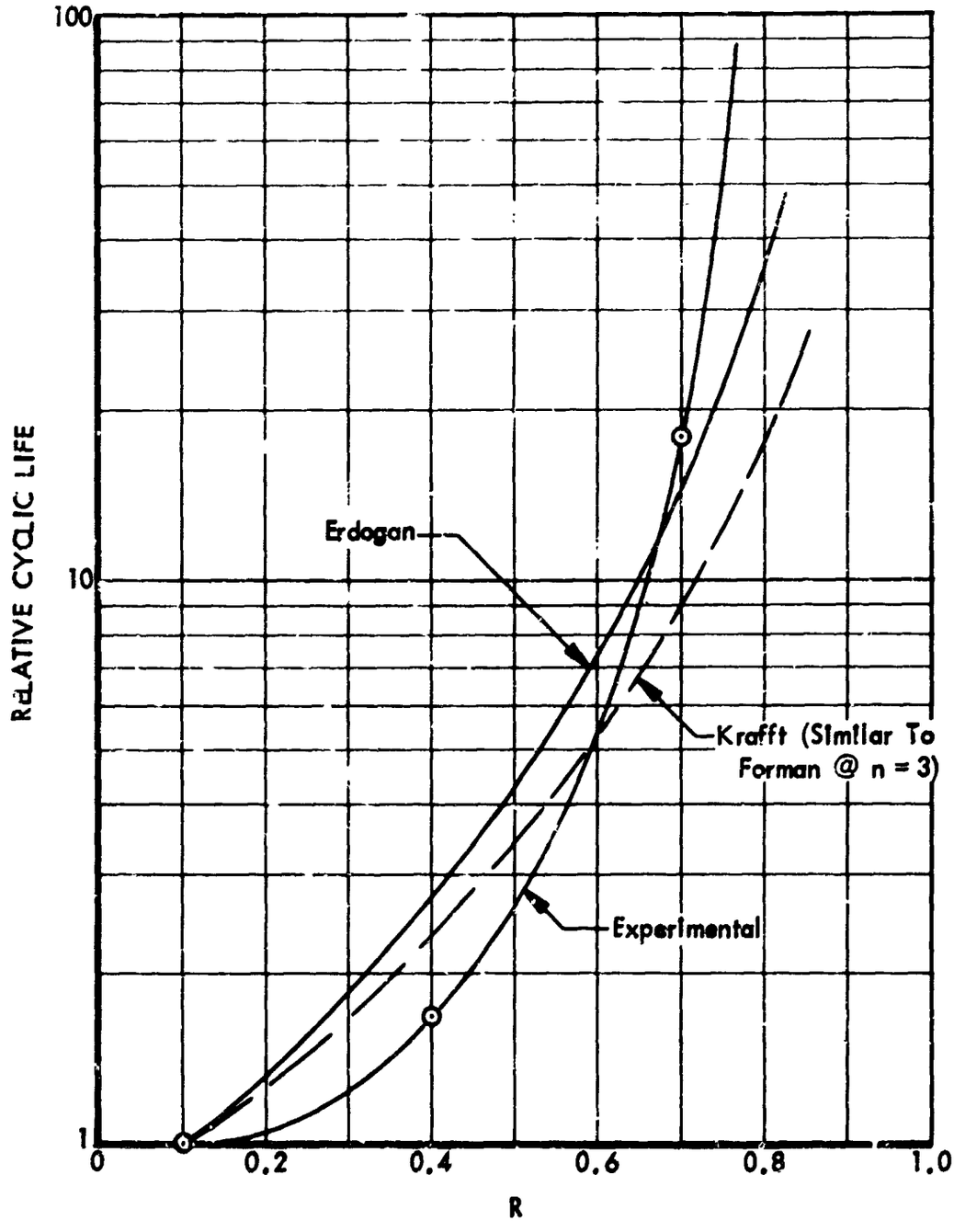

Figure 25: EFFECT OF R VALUE ON CYCLIC LIFE

Table I: AEROJET GENERAL FORGING COMPOSITION
% BY WEIGHT
(Vendor Data)

Al	V	Fe	O_2	C	N_2	H_2
6.1	4.1	0.18	0.17	0.023	0.009	0.007

Solution Treat 1775 °F - 1 Hour - Water Quench
Age 1000 °F - 12 Hours
Stress Relief 1000°F - 4 Hours

Ultimate Strength 174.9 Ksi (Average Of Three Tests)
0.2 % Yield Strength 163.6 Ksi (Average Of Three Tests)

Table II: SUMMARY OF MATERIALS USED AND FRACTURE TESTS PERFORMED

MATERIAL	CYCLIC TESTS IN AIR	STATIC TESTS IN AIR	SUSTAINED LOAD TESTS IN N_2O_4
Aerojet General Cylinder	X	X	
Apollo Fuel Cylinder # 1		X	X
Apollo Fuel Cylinder # 2	X	X	X
Apollo Oxidizer Cylinder # 1	X	X	
Apollo Oxidizer Weld (Segment # 1)	X	X	

Table III: N_2O_4 COMPOSITION[4]

% BY WEIGHT

PROPERTY	SAMPLE "A"	SAMPLE "B"	SAMPLE "C"	SAMPLE "D"
Nitric Oxide	0.31	0.32 [1]	0.52	0.63[2]
Water Equivalent	<0.10	0.013 To 0.12 [3]	<0.10	0.024 To 0.051 [3]
Chloride As Nitrosyl Chloride	ND	0.022	ND	0.020

(1) Original Makeup, Several Additional Analysis Were Taken Later As Follows:
- c) From Test Apparatus; 0.33, 0.33, 0.37%
- b) From Transfer Vessel, After Use; 0.30, 0.34%

(2) Original Makeup, Several Additional Analyses Were Taken Later As Follows:
- a) From Test Apparatus; 0.64, 0.70, 0.74, 0.68%
- b) From Transfer Vessel, After Use; 0.65, 0.53, 0.57%

(3) Several Readings Were Taken DuringThe Course Of Testing. One Value (0.12%) Was Over Spec Limit Of 0.10%, And Was Taken At End Of 120 Hour Specimen Test Run.

(4) Procedures Of MSC-PPD-2A

Table IV: PLAIN STRAIN FRACTURE TOUGHNESS VALUES

MATERIAL	APPROX. SPECIMEN THICKNESS (In.)	AVERAGE STATIC K_{Ic} (Ksi $\sqrt{In}$)	RANGE	NUMBER OF MEASUREMENTS	TEST DIRECTION (2)
Aerojet General Cylinder	0.100	45.8	45.1-46.7	3	L
Apollo Fuel Cylinder #1	0.056	48.6	48.2-49.0	3 (1)	L
Apollo Fuel Cylinder #2	0.056	41.9	39.9-43.0	4 (1)	L
Apollo Oxidizer Cylinder #1	0.065	47.3	47.3	1	L
		43.0	43.0	1	T
Apollo Oxidizer Weld (Segment #1)	0.060	44.7	44.4-45.0	2	T

(1) Includes Two Data Points From Reference 1

(2) 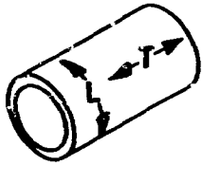

Table V : SUSTAINED LOAD FLAW GROWTH DATA IN N_2O_4
(90 °F Test Temperature)

SPEC.	t In.	W In.	A $In.^2$	a_i In.	$2c_i$ In.	σ_T Ksi	σ_B Ksi	a/Q In.	TEST TIME Hours	TEST TEMP. °F	K_{Ii} Ksi$\sqrt{In.}$	K_{Ii}/K_{Ic}	Δa %	ENVIRON (1)
1-11	0.0564	0.4997	0.0282	0.0245	0.134	86.1	20.6	0.0203	24.3	90	29.0	0.597	0	A
1-12	0.0560	0.5001	0.0280	0.0233	0.129	100.0	20.2	0.0197	23.9	90	32.8	0.675	0	A
2-13	0.0563	0.4987	0.0281	0.0243	0.112	86.8	20.6	0.0187	35.6	90	28.0	0.668	0	B
2-18	0.0563	0.4987	0.0281	0.0268	0.127	92.9	20.5	0.0211	101.3	90	32.0	0.764	19	B
2-9	0.0561	0.4992	0.0280	0.0260	0.127	97.9	20.2	0.0208	23.0	90	33.0	0.788	27	B
2-10	0.0560	0.5000	0.0280	0.0250	0.126	90.0	20.5	0.0200	22.0	90	30.1	0.718	Trace	B
2-11	0.0563	0.4995	0.0281	0.0257	0.126	81.1	21.0	0.0202	22.0	90	27.7	0.661	0	B
1-19	0.0561	0.4982	0.0279	0.0238	0.129	110.0	20.0	0.0203	117.8	90	36.1	0.743	17	B
2-8	0.0561	0.4989	0.0280	0.0245	0.124	87.1	20.5	0.0194	22.2	90	28.6	0.683	0	C
2-7	0.0563	0.4998	0.0281	0.0220	0.126	94.0	20.5	0.0186	22.2	90	29.6	0.706	0	C
1-21	0.0558	0.4988	0.0278	0.0241	0.128	109.0	20.0	0.0203	19.3	90	35.7	0.735	0	C
1-25	0.0557	0.5007	0.0279	0.0264	0.126	110.4	20.0	0.0213	31.3	90	37.7	0.776	15	C
1-122	0.0557	0.4975	0.0277	0.0242	0.127	117.0	19.5	0.0205	19.4	90	38.3	0.788	12	C
1-24	0.0555	0.5008	0.0278	0.0256	0.126	124.1	19.0	0.0215	19.4	90	41.7	0.858	23	C
2-14	0.0555	0.5004	0.0278	0.0247	0.127	91.0	20.4	0.0200	35.4	90	30.2	0.721	0	D
2-31	0.0561	0.4980	0.0279	0.0260	0.127	94.6	20.5	0.0206	117.7	90	32.1	0.766	23	D
1-16	0.0563	0.4987	0.0281	0.0245	0.129	110.0	20.0	0.0206	118.1	90	36.9	0.759	16	D

(1) See Table III For Symbol Explanation

Table VI: SUSTAINED LOAD FLAW GROWTH DATA IN N_2O_4 (70 °F Test Temperature)

SPEC.	t In.	W In.	A $In.^2$	a_i In.	2c In.	σ_T Ksi	σ_B Ksi	a/Q In.	TEST TIME Hours	TEST TEMP. °F	K_{Ii} $Ksi\sqrt{In.}$	K_{Ii}/K_{Ic}	Δa %	ENVIRON (1)
1-9	0.0562	0.4982	0.0280	0.0240	0.129	86.1	20.5	0.0197	21.5	70	28.4	0.584	0	A
1-3	0.0564	0.5000	0.0282	0.0250	0.128	100.0	20.1	0.0204	20.5	70	33.2	0.683	0	A
1-8	0.0561	0.4991	0.0280	0.0230	0.129	112.5	19.5	0.0200	21.6	70	36.5	0.751	0	A
1-26	0.0560	0.4929	0.0276	0.0260	0.126	106.9	19.8	0.0213	21.8	70	36.7	0.755	0	A
1-23	0.0562	0.4947	0.0278	0.0250	0.126	111.8	19.5	0.0207	24.7	70	37.3	0.768	0	A
1-10	0.0563	0.4973	0.0280	0.0240	0.124	126.4	19.0	0.0251	23.0	70	40.9	0.842	Trace	A
1-15	0.0562	0.4985	0.0280	0.0290	0.162	118.9	19.5	0.0253	>.10	70	45.6	0.938	Failed	A
2-12	0.0560	0.4990	0.0279	0.0281	0.129	93.9	20.5	0.0218	20.2	70	33.4	0.797	18	B
2-15	0.0560	0.4997	0.0280	0.0271	0.126	98.9	20.2	0.0213	72.6	70	34.4	0.821	30	B
2-16	0.0563	0.4973	0.0280	0.0250	0.126	92.9	20.5	0.0202	105.2	70	31.0	0.739	0	B
2-17	0.0564	0.4978	0.0281	0.0251	0.125	98.9	20.2	0.0203	105.2	70	32.8	0.783	28	B
1-13	0.0563	0.4987	0.0281	0.0284	0.124	109.6	19.8	0.0219	20.3	70	38.3	0.788	18	B
1-7	0.0563	0.4998	0.0281	0.0260	0.126	117.1	19.5	0.0213	20.2	70	39.3	0.809	8	B
1-14	0.0562	0.5012	0.0282	0.0293	0.125	102.1	20.1	0.0221	20.3	70	36.3	0.747	Trace	B

(1) See Table III For Symbol Explanation

Table VI: (Continued)

SPEC.	t In.	W In.	A $In.^2$	a_i In.	$2c_i$ In.	σ_T Ksi	σ_B Ksi	a/Q In.	TEST TIME Hours	TEST TEMP. °F	K_{Ii} $Ksi\sqrt{In.}$	K_{Ii}/K_{Ic}	Δa %	ENVIRC. (1)
2-2	0.0565	0.5005	0.0283	0.0271	0.128	92.9	20.5	0.0212	21.4	70	32.2	0.768	0	C
1-17	0.0563	0.4975	0.0280	0.0255	0.129	117.0	19.5	0.0213	18.7	70	39.5	0.813	0	C
2-6	0.0563	0.4995	0.0281	0.0226	0.121	109.6	20.0	0.0192	21.9	70	34.7	0.828	22	C
2-5	0.0563	0.4965	0.0280	0.0270	0.128	101.1	20.0	0.0214	21.5	70	35.0	0.835	19	C
1-18	0.0560	0.4995	0.0280	0.0248	0.127	123.9	19.0	0.0212	18.4	70	41.1	0.846	8	C
1-20	0.0558	0.4983	0.0278	0.0244	0.121	130.9	18.4	0.0207	18.4	70	42.6	0.877	8	C
2-29	0.0552	0.4988	0.0275	0.0253	0.127	93.1	20.5	0.0202	22.4	70	31.2	0.745	0	D
2-28	0.0558	0.4997	0.0279	0.0253	0.125	98.9	20.2	0.0205	23.4	70	33.2	0.792	0	D
2-26	0.0564	0.4994	0.0282	0.0280	0.130	105.0	20.0	0.0221	<.10	70	37.1	0.885	Failed	D
2-30	0.0563	0.4979	0.0280	0.0287	0.126	105.0	20.0	0.0220	20.3	70	36.9	0.881	14	D

(1) See Table III For Symbol Explanation

Table VII: CYCLIC FLAW GROWTH DATA FOR AEROJET GENERAL FORGING

R = 0.10 ENVIRONMENT = R.T. AIR

Spec.	t In.	W In.	A $In.^2$	a_i In.	$2c_i$ In.	$\sigma_{max.}$ ksi	a/Q In.	K_{Ii} ksi $\sqrt{in}$	K_{Ii}/K_{Ic}	Cycles To Failure
F1-9A	0.1021	0.8043	0.0821	0.0283	0.131	105.0	0.0221	31.7	0.692	378
J1-7A	0.1027	0.8033	0.0825	0.0290	0.128	105.0	0.0221	31.7	0.692	394
K1-14A	0.1030	0.8046	0.0829	0.0292	0.134	105.0	0.0228	32.2	0.703	384
F1-14A	0.1023	0.8033	0.0822	0.0295	0.133	105.0	0.0229	32.1	0.701	439
I1-6A	0.1026	0.8023	0.0823	0.0301	0.133	105.0	0.0232	32.4	0.707	319
G1-12A	0.1032	0.8064	0.0832	0.0260	0.137	105.0	0.0215	30.9	0.675	475
H1-16A	0.1022	0.8062	0.0824	0.0276	0.133	105.0	0.0219	31.4	0.686	473
H1-1	0.1029	0.8024	0.0827	0.0312	0.131	110.0	0.0235	34.3	0.749	330
F1-2A	0.1023	0.8043	0.0823	0.0326	0.127	110.0	0.0234	34.5	0.753	479
G1-11A	0.1031	0.8049	0.0830	0.0294	0.132	110.0	0.0228	33.7	0.736	306
J1-3A	0.1032	0.8043	0.0830	0.0272	0.135	110.0	0.0221	32.9	0.718	442
I1-9A	0.1030	0.8027	0.0827	0.0314	0.139	110.0	0.0242	35.0	0.764	166
G1-5A	0.1023	0.8053	0.0824	0.0270	0.130	110.0	0.0216	32.1	0.707	329
H1-2	0.1021	0.8023	0.0819	0.0279	0.130	110.0	0.0220	33.1	0.723	329
F1-11	0.1027	0.8011	0.0823	0.0303	0.136	110.0	0.0235	34.1	0.745	320
H1-7	0.1026	0.8000	0.0821	0.0359	0.130	110.0	0.0248	36.1	0.788	161
G1-10	0.1025	0.8005	0.0821	0.0308	0.130	110.0	0.0232	34.1	0.745	363
J1-8	0.1026	0.8029	0.0824	0.0375	0.134	110.0	0.0256	36.7	0.801	199
G1-8	0.1023	0.7998	0.0818	0.0326	0.132	110.0	0.0240	34.9	0.762	207

Table VII: (Continued)

Spec.	t In.	W In.	A In.^{2}	a_i In.	$2c_i$ In.	$\sigma_{max.}$ ksi	a/Q In.	K_{Ii} ksi $\sqrt{in}$	K_{Ii}/K_{Ic}	Cycles To Failure
K1-5	0.1024	0.8014	0.0821	0.0340	0.135	110.0	0.0247	35.5	0.775	161
J1-4	0.1027	0.8020	0.0824	0.0328	0.131	110.0	0.0239	34.9	0.762	328
G1-1	0.1035	0.8026	0.0831	0.0320	0.131	110.0	0.0237	34.7	0.758	324
F1-3C	0.1008	0.8018	0.0808	0.0428	0.177	110.0	0.0318	42.0	0.917	47
F1-4C	0.1014	0.7979	0.0809	0.0393	0.172	110.0	0.0302	40.3	0.879	46
K1-6C	0.1016	0.7971	0.0810	0.0390	0.174	110.0	0.0302	40.3	0.879	44
K1-7A	0.1013	0.0823	0.0813	0.0288	0.131	126.0	0.0230	38.8	0.847	106
F1-12A	0.1011	0.8010	0.0810	0.0319	0.132	126.0	0.0244	40.2	0.878	88
I1-7A	0.1015	0.8010	0.0813	0.0286	0.138	126.0	0.0223	39.1	0.854	111
I1-4B	0.1009	0.8023	0.0810	0.0294	0.119	126.0	0.0221	38.1	0.832	173
K1-12B	0.1014	0.8028	0.0814	0.0247	0.110	126.0	0.0194	35.2	0.769	285
F1-15B	0.1015	0.7998	0.0812	0.0286	0.122	126.0	0.0210	37.1	0.810	194
I1-12B	0.1015	0.8028	0.0815	0.0350	0.119	110.0	0.0232	33.6	0.734	377
F1-5B	0.1009	0.8012	0.0808	0.0340	0.115	110.0	0.0225	33.1	0.723	361
G1-3B	0.1014	0.8042	0.0815	0.0300	0.119	110.0	0.0217	32.8	0.716	403
K1-1C	0.1015	0.7999	0.0812	0.0389	0.181	96.0	0.0302	35.2	0.769	136
K1-6C	0.1012	0.8050	0.0815	0.0315	0.176	96.0	0.0263	31.8	0.694	320
H1-9C	0.1010	0.8026	0.0811	0.0450	0.173	96.0	0.0317	37.0	0.808	177
J1-5A	0.1015	0.7994	0.0811	0.0286	0.130	110.0	0.0223	33.2	0.725	443

Table VII: (Continued)

Spec.	t In.	W In.	A In.^{2}	a_f In.	$2c_f$ In.	$\sigma_{max.}$ ksi	a/Q In.	K_{II} ksi $\sqrt{in}$	K_{II}/K_{Ic}	Cycles to Failure
K1-4A	0.1011	0.8007	0.0810	0.0460	0.150	110.0	0.0296	39.3	0.858	64
I1-2A	0.1012	0.8042	0.0814	0.0298	0.132	110.0	0.0229	33.9	0.740	357
I1-5A	0.1016	0.8005	0.0813	0.0295	0.134	110.0	0.0230	33.8	0.738	294
H1-6A	0.1020	0.7988	0.0815	0.0298	0.137	110.0	0.0233	34.1	0.745	214
J1-1	0.1027	0.8010	0.0823	0.0354	0.129	96.0	0.0241	30.8	0.672	477
G1-4A	0.1017	0.8014	0.0815	0.0322	0.124	96.0	0.0226	29.7	0.648	626
I1-3	0.1028	0.8005	0.0823	0.0303	0.128	96.0	0.0224	29.4	0.642	718

Table VIII: CYCLIC FLAW GROWTH DATA FOR APOLLO FUEL CYLINDER #2

R = 0.10 ENVIRONMENT = R.T. AIR

Spec.	t In.	W In.	A $In.^2$	q In.	$2c_f$ In.	$\sigma_{max.}$ ksi (1)	a/Q In.	K_{II} ksi $\sqrt{in}$	K_{II}/K_{Ic}	Cycles To Failure
2-19	0.0562	0.4984	0.0280	0.0200	0.113	110.0	0.0172	32.5	0.776	71
2-20	0.0550	0.4986	0.0274	0.0224	0.118	110.0	0.0188	34.5	0.823	76
2-21	0.0562	0.4995	0.0281	0.0220	0.128	110.0	0.0193	34.7	0.828	97
2-25	0.0563	0.5007	0.0282	0.0221	0.115	100.0	0.0183	31.0	0.740	160
2-27	0.0562	0.4978	0.0280	0.0225	0.126	100.0	0.0191	31.9	0.761	107
2-24	0.0561	0.4995	0.0280	0.0207	0.110	100.0	0.0172	29.9	0.714	266
2-22	0.0562	0.5005	0.0281	0.0327	0.138	90.0	0.0242	35.7	0.852	18
2-23	0.0560	0.4973	0.0278	0.0290	0.134	90.0	0.0225	32.9	0.785	96
2-32	0.0564	0.4978	0.0281	0.0284	0.130	80.0	0.0217	28.9	0.690	318
2-33	0.0563	0.4996	0.0281	0.0300	0.126	80.0	0.0219	29.3	0.699	234

(1) Max. nominal tension stress (see Figure 13 for corresponding bending stress)

Table IX: CYCLIC FLAW GROWTH DATA FOR APOLLO OXIDIZER CYLINDER #1

R = 0.10 ENVIRONMENT = R.T. AIR

Spec.	t In.	W In.	A $In.^2$	a_i In.	$2c_i$ In.	$\sigma_{max.}$ ksi	a/Q In.	K_{Ii} $ksi\sqrt{in}$	K_{Ii}/K_{Ic}	Cycles To Failure
T-2	0.0647	0.5024	0.0325	0.0245	0.130	104.9	0.0203	31.4	0.730	219
T-3	0.0649	0.5040	0.0327	0.0252	0.125	104.9	0.0204	31.6	0.735	459
T-4	0.0644	0.5042	0.0325	0.0285	0.128	104.9	0.0220	33.7	0.784	150
T-5	0.0647	0.5048	0.0327	0.0288	0.131	104.9	0.0223	34.0	0.791	122
T-6	0.0648	0.8036	0.0521	0.0269	0.126	104.9	0.0211	32.6	0.758	195
T-7	0.0644	0.8039	0.0518	0.0252	0.132	104.9	0.0209	32.1	0.746	495
T-8	0.0649	0.8040	0.0522	0.0251	0.129	104.9	0.0208	31.9	0.741	173
L-2	0.0648	0.5011	0.0325	0.0292	0.128	106.8	0.0223	36.6	0.774	206
L-3	0.0654	0.5028	0.0329	0.0246	0.127	106.8	0.0202	34.4	0.727	315
L-4	0.0649	0.5018	0.0326	0.0268	0.126	106.8	0.0211	35.5	0.751	225
L-5	0.0650	0.5024	0.0327	0.0240	0.127	106.8	0.0199	34.2	0.723	446

Table X: CYCLIC FLAW GROWTH DATA FOR AEROJET GENERAL FORGING

(Reduced Thickness)

R = 0.10 ENVIRONMENT = R.T. AIR

Spec.	t In.	W In.	A $In.^2$	a_i In.	$2c_i$ In.	$\sigma_{max.}$ ksi	a/Q In.	K_{Ii} $ksi\sqrt{in}$	K_{Ii}/K_{Ic}	Cycles To Failure
K1-10A	0.0614	0.8302	0.0509	0.0327	0.127	126.0	0.0240	44.8	0.978	9
G1-6A	0.0608	0.8006	0.0487	0.0277	0.132	126.0	0.0226	41.4	0.904	12
G1-15A	0.0613	0.8009	0.0491	0.0330	0.130	126.0	0.0244	45.4	0.991	6
G1-9A	0.0615	0.8022	0.0493	0.0262	0.131	96.0	0.0210	29.9	0.652	321
I1-13A	0.0624	0.7991	0.0499	0.0246	0.126	96.0	0.0199	28.6	0.624	381
G1-2A	0.0610	0.5010	0.0306	0.0258	0.130	126.0	0.0216	39.7	0.867	56
I1-1A	0.0627	0.5006	0.0314	0.0324	0.133	126.0	0.0245	44.8	0.978	9
G1-16A	0.0623	0.5001	0.0312	0.0300	0.132	126.0	0.0236	42.9	0.937	11
G1-7A	0.0602	0.4998	0.0301	0.0289	0.145	96.0	0.0232	32.4	-	(1)
J1-16B	0.0610	0.4993	0.0305	0.0297	0.114	96.0	0.0208	30.8	0.672	383
G1-13A	0.0611	0.4991	0.0305	0.0272	0.131	96.0	0.0214	30.5	0.666	397

(1) Accidentally overloaded on 3rd cycle.

Table XI: CYCLIC FLAW GROWTH DATA FOR AEROJET GENERAL FORGING

R = 0.40 ENVIRONMENT = R.T. AIR

Spec.	t In.	W In.	A In.^{2}	a_i In.	$2c_i$ In.	$\sigma_{max.}$ ksi	a/Q In.	K_{Ii} ksi $\sqrt{in}$	K_{Ii}/K_{Ic}	Cycles To Failure
F1-10B	0.1031	0.8007	0.0826	0.0255	0.114	126.0	0.0202	35.9	0.784	567
J1-13B	0.1016	0.8002	0.0813	0.0222	0.111	126.0	0.0185	34.2	0.747	512
G1-14B	0.1030	0.8018	0.0824	0.0255	0.114	110.0	0.0197	31.0	0.677	1461
H1-3C	0.1033	0.8017	0.0828	0.0344	0.189	110.0	0.0292	38.7	0.845	371
H1-8C	0.1036	0.8022	0.0831	0.0348	0.180	110.0	0.0288	38.5	0.841	167
I1-11B	0.1030	0.8008	0.0825	0.0277	0.120	110.0	0.0211	32.2	0.703	649
H1-10C	0.1040	0.8016	0.0834	0.0350	0.178	110.0	0.0287	38.5	0.841	279
H1-11C	0.1039	0.8029	0.0834	0.0371	0.181	110.0	0.0299	39.6	0.865	88
H1-15C	0.1037	0.8012	0.0831	0.0298	0.186	96.0	0.0259	31.3	0.683	632
H1-12C	0.1036	0.8020	0.0831	0.0340	0.178	96.0	0.0277	32.9	0.718	484
K1-11B	0.1029	0.8022	0.0825	0.0279	0.118	126.0	0.0215	37.3	0.814	171

Table XII: CYCLIC FLAW GROWTH DATA FOR AEROJET GENERAL FORGING

R = 0.70 ENVIRONMENT = R.T. AIR

Spec.	t In.	W In.	A $In.^2$	a_i In.	$2c_i$ In.	$\sigma_{max.}$ ksi	a/Q In.	K_{Ii} ksi $\sqrt{in}$	K_{Ii}/K_{Ic}	Cycles To Failure
J1-6C	0.1030	0.7994	0.0823	0.0339	0.174	110.0	0.0279	37.8	0.825	1553
J1-15C	0.1020	0.8013	0.0817	0.0402	0.172	110.0	0.0304	40.6	0.886	2190
K1-3C	0.1029	0.8000	0.0823	0.0414	0.171	110.0	0.0308	41.0	0.895	1462
H1-5C	0.1039	0.8011	0.0832	0.0357	0.182	96.0	0.0288	33.7	0.736	5204
H1-4C	0.1030	0.8032	0.0827	0.0331	0.184	96.0	0.0276	32.7	0.714	8199
K1-2B	0.1046	0.8029	0.0840	0.0256	0.124	126.0	0.0211	36.7	0.801	4845
J1-9B	0.1025	0.8016	0.0822	0.0292	0.118	126.0	0.0220	37.8	0.825	1608
J1-11B	0.1031	0.8021	0.0827	0.0247	0.112	126.0	0.0197	35.4	0.773	3894
J1-10B	0.1043	0.8023	0.0837	0.0239	0.111	110.0	0.0188	30.1	0.657	8958
J1-12B	0.1039	0.8012	0.0832	0.0222	0.120	110.0	0.0187	29.9	0.653	6756

Table XIII: CYCLIC FLAW GROWTH DATA FOR APOLLO TANK WELDMENT

R = 0.10 ENVIRONMENT = R.T. AIR

Spec.	t In.	W In.	A $In.^2$	a_i In.	$2c_i$ In.	$\sigma_{max.}$ ksi	a/Q In.	K_{Ii} ksi $\sqrt{in}$	K_{Ii}/K_{Ic}	Cycles To Failure
WA-1	0.0553	0.7066	0.0391	0.0201	0.100	106.0	0.0171	29.0	0.649	1170
WA-2	0.0599	0.7040	0.0422	0.0230	0.101	100.0	0.0181	28.3	0.633	1816
WA-3	0.0618	0.7051	0.0436	0.0210	0.092	100.0	0.0165	26.5	0.593	1692
WB-1	0.0621	0.7028	0.0436	0.0270	0.125	85.0	0.0213	26.9	0.602	2170
WB-2	0.0607	0.7063	0.0426	0.0266	0.118	85.0	0.0205	26.3	0.588	2024
WB-3	0.0601	0.7069	0.0425	0.0237	0.119	85.0	0.0193	25.0	0.559	1800
WB-4	0.0597	0.7037	0.0420	0.0250	0.121	100.0	0.0207	30.9	0.691	802
WB-5	0.0578	0.7028	0.0406	0.0236	0.117	100.0	0.0198	30.0	0.671	1179
WB-6	0.0618	0.7041	0.0435	0.0258	0.118	100.0	0.0208	30.9	0.691	1131
WB-7	0.0662	0.7045	0.0466	0.0262	0.123	118.0	0.0224	37.4	0.837	368
WB-8	0.0624	0.7040	0.0439	0.0250	0.129	118.0	0.0223	37.4	0.837	268
WB-9	0.0598	0.7048	0.0421	0.0258	0.120	118.0	0.0219	37.6	0.841	331
WC-1	0.0571	0.7017	0.0400	0.0294	0.151	118.0	0.0260	43.0	0.962	130
WC-2	0.0612	0.7016	0.0429	0.0313	0.148	118.0	0.0267	43.6	0.975	73
WC-3	0.0614	0.7045	0.0433	0.0290	0.150	118.0	0.0259	41.9	0.937	265

Table XIV: SAMPLE LIFE PREDICTION CALCULATIONS

Specimen G1-13A

$t = 0.0611$ $\sigma = 96$

$a_i = 0.0272$ $2c_i = 0.131$

$a_{cr} = 0.0460$ $2c_{cr} = 0.165$

a In.	a/2c	a/t	Q	a/Q In.	$(a/Q)^{1/2}$ $In.^{1/2}$	M_K	K Ksi $\sqrt{In}$	K_{mean} Ksi $\sqrt{In}$	K_{II}/K_{Ic}	d(a/Q)/dN μ"/Cycle	Δa In.	ΔN Cycles
0.0272	0.208	0.445	1.270	0.0214	0.1463	1.112	30.5					
								31.5	0.688	18.22	0.0028	153.7
0.0300	0.219	0.491	1.300	0.0231	0.1520	1.142	32.5					
								33.7	0.736	26.15	0.0030	114.7
0.0330	0.230	0.540	1.332	0.0248	0.1575	1.180	34.8					
								36.0	0.786	42.86	0.0030	70.0
0.0360	0.241	0.589	1.364	0.0264	0.1625	1.224	37.2					
								38.5	0.840	73.78	0.0030	40.7
0.0390	0.252	0.638	1.398	0.0279	0.1670	1.270	39.7					
								40.7	0.888	133.47	0.0020	15.0
0.0410	0.260	0.671	1.422	0.0288	0.1697	1.308	41.6					
								42.9	0.937	226.78	0.0030	13.2
0.0440	0.271	0.720	1.458	0.0302	0.1738	1.360	44.2					
								45.2	0.987	444.89	0.0020	4.5
0.0460	0.278	0.753	1.480	0.0311	0.1764	1.400	46.2					
											$\Sigma N =$	411.8